Chapter 4
Mechanics for Fluidics and Bio-Devices

Luis Guillermo Villanueva, Annalisa De Pastina and Magalie Faivre

Abstract In this chapter, we firstly present mechanical elements which are essential components of Lab-On-Chip devices as they can provide sensing, mixing, pumping and controlled delivery of small fluidic volumes. Microvalves, crucial for the on-chip implementation of complex fluidic patterns, are discussed first. Micropumps, typically built as a collection of microvalves operated in sequence, are subsequently described. Finally, a short overview of nanomechanical biosensors, which have demonstrated great capabilities in label-free sensing applications, is provided. Particular attention will be paid to mechanical sensing in liquids, focusing on limitations and novel techniques. In a second part, we will focus on concentrating, focusing, trapping, sorting and single cell biomechanical characterization which are critical steps in various biomedical applications such as diagnostics, therapeutics, drug screening and cell biology. Microfluidic technologies propose attractive engineered microenvironments for the manipulation and the study of cellular mechanics compatible with high throughput. The different approaches available to act on cells and perform mechanical phenotyping in microsystems are detailed and discussed.

Keywords Microvalves · Micropumps · Nanomechanical sensors · Cell manipulation · Cell biomechanics · Passive microfluidics · Microfluidic deformability assays

L. G. Villanueva · A. De Pastina
EPFL-STI-IGM-NEMS, Station 9, ME D2 2726, CH-1015, Lausanne, Switzerland
e-mail: guillermo.villanueva@epfl.ch

M. Faivre (✉)
Institut des Nanotechnologies de Lyon INL-UMR5270, CNRS, Université de Lyon, Université Lyon 1, Villeurbanne 69622, France
e-mail: magalie.faivre@univ-lyon1.fr

G. Barbillon et al. (eds.), *Engineering of Micro/Nano Biosystems*, Microtechnology and MEMS, https://doi.org/10.1007/978-981-13-6549-2_4

4.1 Introduction

Mechanics and biology seem at first view rather remotely related fields but as demonstrated in this chapter, mechanics, fluidics and biology can be nicely combined to control fluids, to manipulate and sort cells and to perform biodetection. In the following sections, microcomponents for fluidics, passive microfluidics and mechanics for biodevices will be successively reviewed:

Macroscale mechanical pumps and valves can be used for fluid injection and distribution in microchannels. However, their miniaturization is finally desirable to get fully integrated micro/nano biosystems that are portable and more autonomous. As detailed in Sect. 4.2 of this chapter, a large variety of microvalves and micropumps were proposed and developed for this purpose.

The development of atomic force microscopy and of micro/nano-electromechanical systems (M/NEMS) in the last three decades clearly demonstrated the high sensitivity of micro/nano-mechanical structures such as cantilever micro/nano-beams, micro/nano-bridges, membranes… and of acoustic microdevices to added mass, to mechanical stress or/and to tiny forces. Their potential for biodetection began to be investigated around year 2000 and some typical examples of biomechanical detection are reviewed in the last part of Sect. 4.2.

Micro/nano bio system can also take benefit of mechanics for cell manipulation, sorting and analysis owing to the similar size of fluidic microchannels and of cells, and to the variability of cell density and mechanical properties. The various ways to apply passive microfluidics to cells manipulation and to perform mechanical characterization of cells by the way of microfluidics are described in Sects. 4.3 and 4.4.

4.2 Mechanical Microcomponents for Fluidics (Annalisa De Pastina and Luis Guillermo Villanueva)

Micro- and nano-electromechanical systems (M-NEMS) are defined as electrically transduced continuum mechanical structures, such as beams, strings, plates, or membranes, with dimensions in the order of micrometers. What started being a very efficient solution for inertial sensing in the automotive industry has expanded to numerous different applications, including playing a fundamental role in miniaturized microfluidic devices [1, 2]. Indeed, mechanical elements are essential components of Lab-On-Chip devices as they can provide sensing, mixing, pumping and controlled delivery of small fluidic volumes.

This part of the chapter focusses on *Microvalves*, *Micropumps*, and *Nanomechanical biosensors*, as they are the main types of components required for fully integrated microfluidic systems.

- *Microvalves* control routing, timing, and separation of fluids within a microfluidic device and are crucial for the on-chip implementation of complex fluidic patterns.
- *Micropumps* generate temporal and volumetric flow and allow reducing the amount of external hardware necessary to operate a microfluidic device.
- *Nanomechanical biosensors* have demonstrated great capabilities in label-free sensing applications, such as detection of viruses and single molecules [3].

In the following paragraphs microvalves are discussed first, followed by micropumps, since many micropumps are built as a collection of microvalves operated in sequence. These two broad categories are further subdivided into several types. Each type inherently possesses many strengths and weaknesses which must be considered when choosing an appropriate solution for a given application. Finally, a short overview of nanomechanical biosensors operating in static and dynamic mode is provided. Particular attention will be paid to mechanical sensing in liquids, focusing on limitations and novel techniques.

4.2.1 Mechanical Microvalves

Microvalves can be divided in three major types: active (internal and external), and passive. *Active* microvalves have in common an actuating element (the different kinds are analyzed below) to stop or allow the flow. Active microvalves can be classified depending on whether the actuator is external (e.g. built-in modular or pneumatic) or the actuator is integrated on the microfluidic chip using MEMS-based technologies (e.g. magnetic, electric, piezoelectric or thermal actuators). Internal valves offer high performances, but also high complexity and fabrication costs. In contrast, external valves are cheaper and simpler, but the final solution is bulky, not viable for miniaturization. *Passive* valves, sometimes called check-valves, do not include actuation, they open to forward pressure showing a diode-like behavior.

Microvalves' applications include flow regulation, on/off switching and sealing of liquids, gases or vacuum. The desired characteristics of an ideal microvalve include no leakage flow, reduced dead volume, reduced power consumption, large pressure resistance, fast response time, insensitivity to contamination, ability to operate both with liquids and gases, low complexity, low fabrication cost, and disposability [4]. Unfortunately, up to date there is no valve technology or design that simultaneously satisfies all these requirements. Therefore, the most appropriate type of microvalve will change according to the demands of a specific application.

4.2.1.1 Active External

External active microvalves are actuated by the aid of external systems such as built-in modular or pneumatic means. This approach suffers, logically, from difficulties in miniaturization, given the fact that additional components are required, like air/vacuum pumps or solenoids. However, external microvalves exhibit no leakage flow even at high input pressures and excellent performances in on/off switching or sealing.

Two main categories can be distinguished, namely *modular* and *pneumatic* external valves. *Modular* external microvalves include built-in [5] or rotary configurations [6]. Microvalves actuated by an external *pneumatic* system are distinguished between membranes [7] and in-line [8].

Quake et al. presented an *in-line pneumatic valve* system consisting of a crossed-microfluidic PDMS channel block, sealed to glass or elastomer substrate, as shown in Fig. 4.1a. An actuation channel is filled by pressurized gas allowing a thin membrane to deflect and close the bonded fluidic channel. Two different configurations have been demonstrated and compared, as presented in Fig. 4.1b, c.

The push-down configuration (Fig. 4.1b) consists of 100 µm wide and 10 µm thick channels with a minimum actuation pressure of 40 kPa to seal the fluidic channel [8]. The second valve generation, push-up configuration (Fig. 4.1c), allows an increase fluidic channel height up to 55 µm, and a lower valve actuation pressure of 15 kPa [9].

The push-up membrane was further improved by Pandolfi and Ortiz. They demonstrated that the channel closure can be assisted by out-of-plane buckling of the membrane caused by controlled chemical swelling in silicone oil. This strategy allowed them to decrease the actuation pressure down to 8 kPa [10].

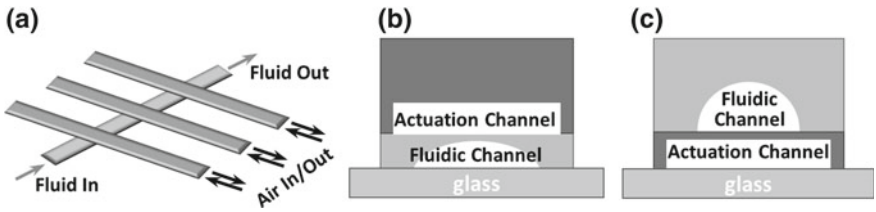

Fig. 4.1 **a** 3-D representation of three in-line valves with individual control proposed in [8]. **b** Push-down valve geometry. A curved membrane of variable thickness is deflected by applying pressure to close the channel underneath. This configuration requires high aspect ratio fluidic channels. **c** Push-up valve configuration. A membrane of uniform thickness is deflected when pressure is applied in the actuation channel to close the fluidic channel on top. The pressure applied in this case is not dependent of the aspect ratio of the fluidic channel

4.2.1.2 Active Internal

As opposed to the previous type of valves, it is also possible to have the actuation mechanism integrated on-chip. In those cases, the moving component is usually a membrane. Various actuation principles can be adopted to actuate mechanical moving parts and the actuators are integrated in the valve structure itself.

Mechanical active microvalves have two main disadvantages: unavoidable leakage flow and relatively high cost due to their complicated structure. While leakage flow is a critical feature for on/off switching applications, it is less critical for flow regulation. Therefore, micromachined active microvalves are usually preferred for gas or selected liquid regulation, even though numerous on/off switching applications have been reported [11]. Due to their elevated cost, internal active microvalves are mainly reusable and are usually implemented in non-disposable devices.

The following paragraphs provide a brief analysis of mechanical active microvalves, classified according to their actuation principle. Bear in mind that we do not intend to do a thorough review of these actuation principles, just introducing them succinctly.

Electromagnetic

A wire carrying a current in the presence of a magnetic field will experience the Lorentz force $\vec{F}_{em} = (\vec{I} \times \vec{B})L$, where $\vec{F}_{em}$ is the electromagnetic force, $\vec{I}$ is the current through the wire, $\vec{B}$ is the magnetic field and L is the wire length. The magnitude of the force, $|\vec{F}_{em}|$, scales down with dimensions $\propto l^{\alpha}$, with α between 1 and 2, if we consider an external magnetic field, and depending on whether we take constant current, voltage or power [12]. In any case, this scaling shows that for very small sizes the force is compromised.

Electromagnetic microvalves operate at low voltages and are able to generate large actuation forces (see Fig. 4.2a). However, electromagnetic actuators require an external magnetic field, thus rendering them difficult to miniaturize, even though in some cases they have been shown to be integrated [13]. As current needs to be sent through the wires, electromagnetic microvalves exhibit high power consumption and high heat dissipation [14].

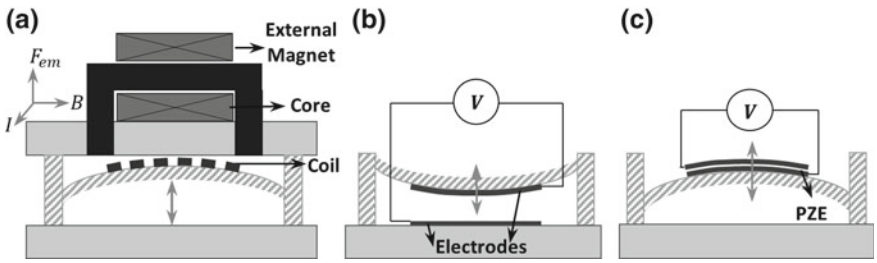

Fig. 4.2 General schematic of three different actuation principles for active internal microvalves: **a** electromagnetic, **b** electrostatic, and **c** piezoelectric

In 1979 Terry et al. proposed the first active micromachined valve, using a solenoid plunger, which was physically connected to a 100 nm thick nickel membrane. The normally closed microvalve constituted a component of an integrated gas chromatography system [15].

Electrostatic

Electrostatic actuation is based on the Coulomb attraction force between oppositely charged plates. Assuming a system with two parallel plates and a voltage difference (V) is set between them, the force takes the form: $F_{es} = -\frac{1}{2}\frac{\varepsilon_0 \varepsilon_r A V^2}{x^2}$ where $\varepsilon_0 \varepsilon_r$ is the dielectric constant, A the electrode area, and x the electrode spacing. Due to the scaling of the electrostatic force, $F_{es} \propto l^0$, the miniaturization of electrostatic actuators is much simpler than electromagnetic ones.

In electrostatic microvalves, one of the electrodes to give rise to the force is typically located on the membrane, whereas the second one is typically placed on the substrate, within the microchannel to be closed or opened, as presented in Fig. 4.2b. This type of valves has a fast response time and low power consumption in the order of 1 mW, since almost no current flows through the system. The main limitation is the small achievable displacements, usually in the order of few micrometers.

Modifications of the basic schematic shown in Fig. 4.3 have been proposed in several ways. The efficiency of the system can be improved using S-shaped membranes that move back and forth (laterally) instead of up and down [16]. Different materials have been used for the fabrication of the actuation membrane: flexible materials as polymide [17], requiring lower actuation voltages, and rigid silicon membrane [18, 19], preferred for high pressure control.

Piezoelectric

Piezoelectricity is the property of a material to respond with a mechanical deformation (ε_j) to an applied voltage. We consider a piezoelectric layer of width w_{PZE}, thickness t_{PZE}, Young's modulus E_{PZE} and piezoelectric coefficients d_{ij}. Applying an electric voltage across the thickness of the piezoelectric layer (V) causes a deformation in the piezoelectric layer and therefore a force (assuming a structure working in pure elongation), $F_{PZE} = E_{PZE} \cdot d_{33} \cdot w_{PZE} \cdot L_{PZE} \frac{V}{t_{PZE}}$ and scales as l. Although large force and fast response time are achieved through piezoelectric actuators, small strokes and complexity in the fabrication are challenging issues.

The drawback of small strokes has been overcome via different alternatives as the hydraulic amplification of the piezoelectric deflection [20], stacked piezoelectric

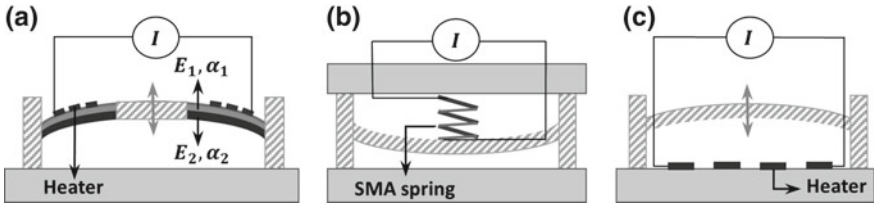

Fig. 4.3 Schematic representation of three different thermo-mechanical actuation principles: **a** bimetallic, **b** shape memory alloy, and **c** thermopneumatic actuation

disks [21] or piezo bimorphs, presented in Fig. 4.2c (i.e. structures working in flexion instead that elongation) [22, 23].

For example, Rogge et al. proposed a hydraulic transmission system, which is able to translate a small-scale deflection of the piezodisk into a larger movement of a valve membrane, showing an increase of the membrane displacement up to 25 times, achieving a valve stroke of 50 μm [24].

Thermal

Thermo-mechanical actuation is based on the expansion caused by a change in temperature in either the mechanical structure (bimetallic effect and shape memory alloys) or its surroundings (thermopneumatic). In general, thermal actuation provides large strokes and large actuation forces, but this comes with a slow response time and a high power consumption.

Bimetallic

Bimetallic actuation, schematically represented in Fig. 4.3a, is based on the difference of thermal expansion coefficients of multiple materials bonded together. When a multilayer stack of dissimilar materials, not necessarily metals, is subjected to temperature changes (ΔT), thermal stresses (σ_i) are induced in each material: $\sigma_i = E_i \cdot \alpha_i \cdot \Delta T$, where E_i is the Young's modulus of material i. This stress distribution translates into bending of the structure [25]. Among thermal microvalves, bimetallic actuated ones exhibit the lowest power consumption.

Shape Memory Alloy (SMA)

Shape memory alloy (SMA) actuated microvalves make use of the shape memory effect in SMAs such as Au/Cu, In/Ti and Ni/Ti. These materials can be easily deformed at room temperature, but they recover their pre-deformed shape when heated up above a phase transition temperature, which is characteristic of each material. This phase transition results in mechanical deformation that is used for actuation [26], as shown in Fig. 4.3b.

As an example, we can take the case of Kohl et al. who developed normally open gas microvalves actuated by microfabricated SMA thin films of NiTiPd. The main components are a polyimide membrane, a spacer and the SMA device. They demonstrate control of pressure differences below 250 kPa, corresponding to a gas flow of 360 mL·min^{-1} with a stroke of about 20 μm [27].

Thermopneumatic

Thermopneumatic actuation is based on thermally induced volume change and/or phase change of fluids sealed in a cavity with at least one compliant wall (Fig. 4.3c). For liquids, the thermally induced pressure increase is related to the thermal expansion coefficient, and the temperature increase. Since the actuation force is given by $F_{tp} = P \cdot A$, the thermopneumatic force is related to the surface A of the moving membrane, thus it scales as the square of the size. Thermopneumatic actuation combined with soft materials is very promising to achieve large actuation force and large stroke, with however a large power consumption. An example is reported from Takao et al. [28], presenting a thermo-pneumatic in-channel PDMS

microvalve applicable to integrated blood test system. The microvalve consists of two separated chambers and a PDMS diaphragm actuated by pneumatic pressure controlled by an integrated Au microheater.

Bistable

As opposed to what we have seen till now, this refers more to a design choice, rather than to an actuating mechanism. Power consumption is one of the major factor of interest when choosing the suitable microvalve for a specific application. Any of the actuation mechanisms shown till now might need to have a continuous application of power to keep the microvalves open or closed. This limitation can be overcome through the design of bistable structures that only require power during the transition between two stable positions, regardless of the actuation principle (Fig. 4.4).

Bistable microvalves have been reported using thermal buckling of membranes [29], pneumatic switching actuation [30], and combination of multiple actuation principles [31, 32].

An example of thermal buckling is reported by Goll et al. [29]. The authors use a polyimide membrane which buckles due to a compressive stress induced by thermal treatment and mechanical loading. Because of the bistability of the microvalve, only a short pressure rise and a short pressure drop are obtained by controlling an electric current through a resistive heater in the actuator chamber.

4.2.1.3 Passive

While active valves control flow rate through pressure differences and have complex structures due to their various actuation principles, passive valves (check valves) only open to forward pressure and have simple structures, showing diode-like characteristics. The valving efficiency of passive valves is relatively poor, since the performance of these check valves depends on input pressure. This lack of efficiency results in leakage flows at low pressure. Despite this drawback,

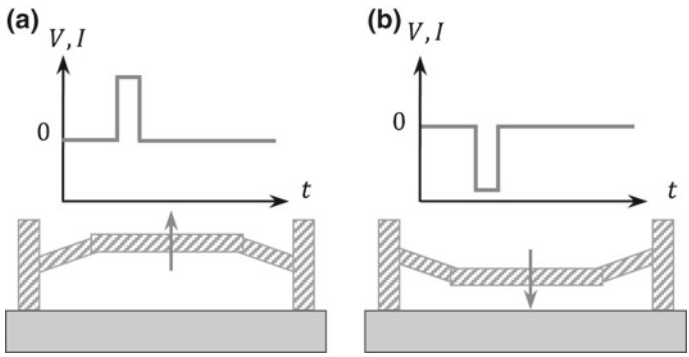

Fig. 4.4 Schematic representation of the actuation principle of bistable microvalves

most passive microvalves are incorporated as check valves in inlets and outlets of reciprocal displacement micropumps. The mechanical moving component can be constituted of a cantilever (flap type), a membrane or a ball, as shown in Fig. 4.5.

In case of disposable microfluidics, irreversible *burst valves* are highly preferred, due to their single-use nature and simple fabrication [33].

Flap and Membrane

Flap and membrane valves usually have a mechanical component that forms a seal with the valve seat, allowing fluid flow only in one direction and preventing reverse flow.

Voldman et al. successfully developed a silicon flap microvalve, placed at the end of a silicon nozzle, to control biochemical reactions of two compounds [34]. However, the use of a rigid material as silicon can represent a limiting factor, since stiction between the moving parts can occur, and even slight contaminations can affect the integrity of the sealing. Such limitations can be overcome by the use of soft materials like PDMS or hydrogels, which are not only flexible, but also cheaper and biocompatible [35]. On the other hand, PDMS, polymide and hydrogels tend to leak liquid and gases due to their high permeabilities. Therefore, parylene is often chosen as valve material, because of its low permeability to liquids and low Young's modulus. As an example, Kim et al. reported in [36] the fabrication of two different configurations of parylene micromechanical check valves: cantilever-type flap valve and bridge-type membrane valve. In both cases, one valve controls the flow in one direction, while the other controls the flow in the opposite direction.

The main difference between the flap-type and the membrane-type configuration lies in the relative movement between the fluid and the mechanical part of the valve. For the cantilever-type flap valve, the flow going through the valves produces rotating motion of the valves and induces turbulences in the flow around the valve opening ends. For the bridge-type valve, the flow can go through the valve with a symmetrically distributed velocity profile.

Ball

Ball valves allow the control of a unidirectional flow. The working principle is very similar to flap and membrane valves, but the mechanical moving element in this case is a microsphere.

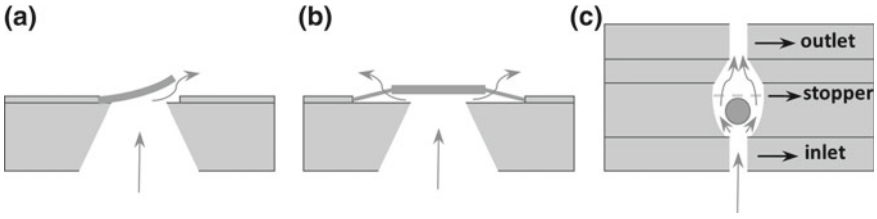

Fig. 4.5 Simple representation of passive microvalves, where the mechanical moving component can be either a cantilever (**a**), a membrane (**b**), or a ball (**c**). In case of ball microvalves a stopper is needed in order to keep the ball confined in his cavity and allow the valve opening. The blue arrows represent the direction of the flow

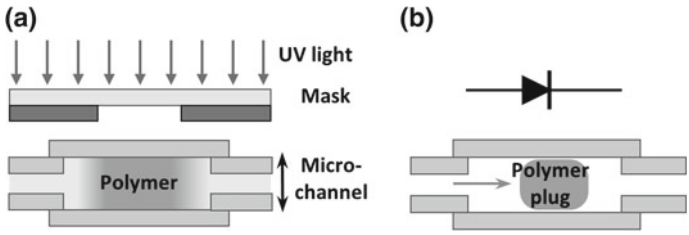

Fig. 4.6 **a** Schematic of photopolymerization method for the fabrication of mobile piston in microchannels. **b** The resulting diode-like polymer plug is shown

Ball valves historically find their main application in heart valve prosthesis. In 1954, Hufnagel et al. treated patients with aortic insufficiency with insertion of an acrylic ball valve into the descending aorta [37], while in September 1960, Starr-Edwards performed the first successful mitral valve replacement using a caged-ball valve [38, 39].

Miniaturization of these valves allowed their use as passive check valves in micropump structures, as will be described in Sect. 4.2.2 Mechanical Micropumps.

In-line Polymerized Gel Mobile Structure

In-line polymerized gel microvalves are a particular example of ball valves. They use in situ UV or visible light induced photopolymerization to create gel plugs and interrupt liquid flows, working as diode-like mechanical components (Fig. 4.6a and b).

Photopolymerization is induced by selectively exposing the chip to UV light, in order to define mobile pistons inside the microchannels. After UV exposure, the unwanted polymer can be flushed away with organic solvents while sealing or confining surfaces prevent the moving part from flowing out when pressure is applied. The main advantage of this technique is the simple fabrication that does not require any sacrificial material or mechanical assembly.

Hasselbrink et al. used photopolymerization of Teflon-like polymer to fabricate micropistons in microfludic channels, demonstrating sealing pressures up to 30 MPa [40]. Another example is given by Seidemann et al. who fabricated SU8 photoepoxy triangular check valve, anchored to a S-shaped spring [41].

4.2.2 Mechanical Micropumps

Micropumps generate temporal and volumetric flow and allow to reduce the amount of external hardware necessary to operate a microfluidic device. They find application in many different fields such as microfluidic transport, microelectronic cooling, micropropulsion for space exploration, dispensing therapeutics, and single cells monitoring [42–45].

In essence, pumps are smart combination of valves (both active and passive) that put fluid in motion. Pumps may be classified based on the applications they serve, the materials from which they are constructed, the liquids they handle, and even their orientation in space.

We adopt here a more basic classification system according to the way by which micropumps induce fluid flow and pressure [44, 46]. This classification is thus related to the pump itself and is independent of any consideration external to the pump or even to the materials from which it is constructed. Under this classification criterion, all pumps are divided into two major categories: dynamic micropumps and displacement micropumps.

Displacement micropumps exert pressure forces on the working fluid through one or more moving boundaries. Mechanical microvalves are typically used as a constitutive part of displacement pumps.

Dynamic micropumps continuously add energy to the working fluid in order to increase its pressure directly or indirectly through its momentum. Momentum added to the fluid in a displacement pump can subsequently be converted into pressure by the action of an external fluidic resistance.

Several parameters need to be taken into account in order to optimize the micropump performances. Some of them are reliability, power consumption, cost, miniaturization, biocompatibility, and efficiency. This latter concept, pump efficiency η, is defined as the ratio of the power delivered to the fluid by the pump P_{pump} and the power required to drive the pump actuator $P_{actuator}$. In an ideal pump, P_{pump} and $P_{actuator}$ are identical as no losses exist. In a real pump three sources of losses can be distinguished: fluid leakage losses (volumetric efficiency η_V), frictional losses (mechanical efficiency η_M), and losses due to imperfect pump construction (hydraulic efficiency η_H). Therefore, the total pump efficiency can be written as follows: $\eta = \eta_V \eta_M \eta_H = P_{pump}/P_{actuator}$ [42].

4.2.2.1 Displacement

Displacement micropumps can operate in a periodic or aperiodic manner. Periodic displacement micropumps give a continuous motion to the fluid, and can be divided into reciprocating and rotary types, depending on the nature of movement carried out by the pressure-producing mechanical element. Aperiodic displacement pumps do not typically involve the movement of any mechanical parts and so they are not going to be studied here, but the interested reader can further read about them in [44].

Reciprocating: Diaphragm

The majority of reported micropumps are reciprocating displacement pumps in which the moving surface is a diaphragm, also called membrane pumps or diaphragm pumps. Alternatively the moving mechanical element can also be constituted by a piston [44].

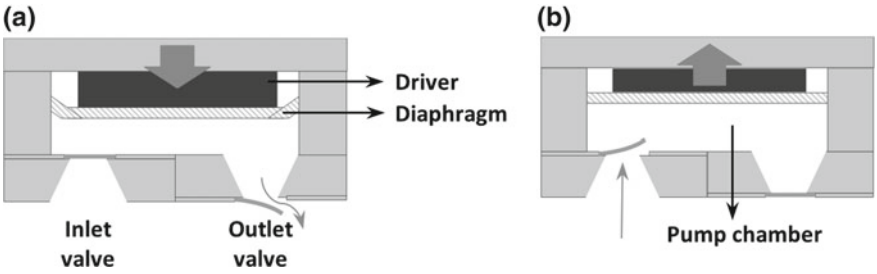

Fig. 4.7 Structure and operation of a typical reciprocating displacement micropump. During operation the driver acts on the pump diaphragm to alternately increase and decrease the pump chamber volume. Fluid is forced out of the pump chamber through the outlet check valve, during the discharge stroke (**a**). During the suction stroke fluid is drawn in through the inlet check valve due to the pump chamber expansion (**b**)

The basic components of diaphragm pumps are shown in Fig. 4.7, and are a pump chamber, an actuator mechanism or driver and two passive check valves. Richter et al. have demonstrated that the maximum pressure p_{max} produced by reciprocating displacement micropumps is inversely dependent of the fluid compressibility κ, consequently these devices are generally capable of achieving higher pressures with liquid-phase working fluids better than with gas phase [47]. Complications may arise due to the presence of air bubbles in the working fluid, which would increase its compressibility, decreasing p_{max}. Therefore, susceptibility to bubbles is a significant problem for reciprocating displacement micropumps.

The most common method for fabricating micropumps is micromachining of silicon combined with glass bonding layers. The first silicon micropump was proposed by Van Lintel et al. [48] in 1988, and consisted of a single-chamber reciprocating displacement silicon micropump, driven via piezoelectric disk actuator placed on top of a glass diaphragm. While most micropumps presented in literature have a single pump chamber, a few micropumps have been reported with multiple chambers. One example is given by Smith et al. who fabricated a reciprocating displacement micropump with three chambers in series, piezoelectrically actuated and requiring no valve to rectify the flow [49]. Also, Shoji et al. proposed a reciprocating displacement microvalve with two pump chambers arranged in parallel, showing a continuous and rippleless flow in the pump output [50].

Actuation within the pump has been reported to be of many different types, including every single case analyzed in the previous paragraph. Thus, the same advantages and limitations discussed for microvalves are still valid for micropumps.

Pump diaphragm material must be chosen according to the frequency range of actuation and fluid properties. For micropumps driven by low frequency and/or low force actuators, a low elastic modulus diaphragm material, such as silicone rubber, generally allows to maximize the pump stroke volume, thus positively impacting device performances [51]. However, the high permeability of soft polymers to liquids may be a concern depending of the application. On the other hand, the fast

mechanical response of a stiff diaphragm generally yields the best performance in case of drivers operating at high frequencies. For example silicon and glass are the most common diaphragm materials in piezoelectric driven reciprocating displacement micropumps.

Rotary

A small number of microscale displacement pumps employ rotary elements such as gears or vanes for generating fluidic flow. Based on different design concepts, rotary micropumps make use of either viscous forces or pressure forces to carry out the pumping action [52].

Ashouri et al. proposed a novel high-efficiency prototype microfluidic pump that uses magnetic properties of a ferrofluid in both pumping and valving mechanisms, presented in Fig. 4.8. A cylindrical magnetic piston covered by ferrofluid functions as a revolving element which sweeps the perimeter of the cylindrical pumping chamber. The piston is externally actuated by a motorized off-center permanent magnet. Ferrofluid is used to cover the gaps between the magnetic piston and the channel walls, also serves as a separating plug between the inlet and the outlet of the chamber preventing recirculation of the pumped fluid inside the chamber. This novel revolving piston design eliminates the need for an inlet valve, while a ball passive valve is placed at the outlet of the pump [53].

Key issues for such pumps include ensuring the immiscibility of the ferrofluidic plug and liquid being pumped, degradation of the ferrofluid over time, and the need to incorporate an external controller for the magnet.

Another interesting example of rotary displacement micropump is the one proposed by Chou et al. They used a microfabricated rotary pump to demonstrate active mixing of biological entities, overcoming their slow diffusion process [54]. Because microfluidic devices operate at low Reynolds number, many fluidic

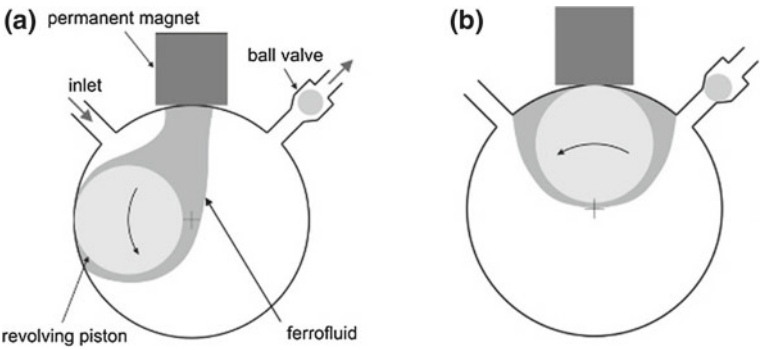

Fig. 4.8 Cross section and working principle of rotary micropump proposed by Ashouri et al. When the revolving piston is sweeping the larger sector between the inlet and the outlet ports (**a**) the counter clockwise displaced volume of the working fluid will be pushed into the outlet port. When instead the magnetic revolving piston is confined to the small sector between the inlet and the outlet ports (**b**) the check valve located at the outlet will prevent the fluid from flowing reversely from the outlet port to the inlet port [53]

operations are limited by diffusion in laminar flow. An active mixing apparatus takes much smaller area and thus saves the amount of time required and of precious reagents used, compared to a long narrow channel.

4.2.2.2 Dynamic

Dynamic micropumps require continuous addition of energy to the working fluid, in order to increase its pressure directly or indirectly through its momentum. Momentum added to the fluid in a displacement pump can then be converted into pressure by the action of a change in the fluidic resistance. These pumps generate a continuous flow without pulsation, and are simpler to fabricate than displacement micropumps. Typically, dynamic micropumps have no mechanical moving parts, and are based on non mechanical physical principle, which does not belong to the intent of this paragraph [44]. However, dynamic micropumps based on ultrasonic flexural plate waves and surface acoustic waves have been reported, which allow for directed flow in simple microchannels with no valves or other moving parts.

Acoustic

The use of mechanical actuation for fluidic pumping requires the use of sophisticated and often costly fabrication processes to develop the device and its micromachined moving parts.

Tovar and Lee demonstrated a novel and simple method for pumping and mixing fluids within a microfluidic system using an acoustic energy source, namely a piezoelectric (PZT) buzzer. Such device, termed lateral cavity acoustic transducer (LCAT), is based on the principle of acoustic microstreaming: air bubbles trapped in lateral cavities adjacent to the microfluidic channels are excited by an external acoustic field, which causes the air/liquid interface to vibrate. This energy is then passed to the bulk liquid and produces a net force perpendicular to the bubble interface and out the end of the cavity, as shown in Fig. 4.9. The pumping flow rate generated by the cavities is controlled through adjusting the amplitude and frequency at which the PZT is driven and also by determining the optimal bubble

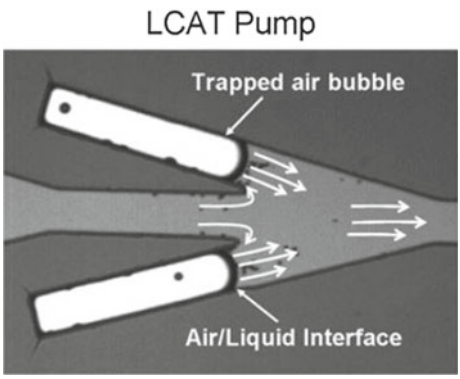

Fig. 4.9 Micrograph of the lateral cavity acoustic transducer micropump design. The microfluidic channel is 100 μm wide [55]

trapping angle. The maximum flow rate was obtained with an angle of 15° between the lateral cavity and the microfluidic channel [55].

Mixing of beads and cells into downstream microchannels has also been demonstrated by simply placing the air bubble cavity perpendicular to the microfluidic channel, which results in a drag force deflecting the particle in the direction perpendicular to the bulk flow [56].

The main advantage that the LCAT device has over other pumping methods is the ease of operation and fabrication. However, the classical configuration of closed channel networks can present several disadvantages. In pumping biological molecules and cells there is concern over reagent loss by adhesion to the wall, and clogging of small channels. Also, the pressure required to move a liquid confined into a microfluidic channel scales inversely with the channel dimension [57]. This means that the power of the pumps has to be increased by the same factor the channel size is reduced, which complicates the scaling and the integration into a portable system.

An alternative to the common closed microfluidic networks is given by the *surface acoustic waves* (SAW) technology [43], that will be discussed in more detail in the following paragraph, and that can be applied to fluidic volumes from few picoliters up to several microliters. A representative example of SAW microfluidic actuation is provided by Guttenberg et al. [58], who proposed a microfluidic device for on-chip PCR, operating at a planar open surface. In such device the fluid is transported on a piezoelectric substrate, and in order to prevent evaporation of the PCR reagents at high temperatures the fluidic sample is enclosed in droplets of mineral oil that can be ultrasonically actuated along the surface plane. Actuation of small droplets on the surface of a SAW chip is caused by the effect of acoustic streaming. This phenomenon appears when intensive sound fields are travelling through a liquid. The viscosity of the medium attenuates the amplitude of the acoustic waves during its propagation, which leads to a pressure gradient in the liquid. If the gradient is large enough, the fluid starts to move in the same direction as the sound wave. The RF power threshold for the movement strongly depends on the contact angle of the droplets. Therefore, the distribution and the motion of the fluid on the surface is controlled mainly by the surface free energy, which makes surface contamination a sensitive concern in SAW microfluidic actuation.

4.2.3 Mechanical Biosensors

Micro- and Nano-mechanical biosensors are mechanical transducers with micro- and nano-sized moving parts. Their fabrication relies on the standard semiconductor processing techniques, enabling for efficient batch production. Nanomechanical biosensors are usually cantilever-shaped, but can also include doubly-clamped beams, membranes, and SAW or BAW (bulk acoustic waves) devices.

Robust and well-established electrical and optical sensors still dominate the field of biological detection in terms of market share. However, in the past two decades

Micro and Nano Mechanical systems (N/MEMS) have been receiving a lot of attention at the research level. The main reason for this development of N/MEMS in life-science applications (BioMEMS) has been to address the *mechanical nature* of many fundamental biological processes. A clear example is cell mechanical properties such as stiffness or viscoelasticity, which represent a valid diagnostic biomarker for several pathologies like cancer, malaria and sickle cell anemia among others [59, 60]. In addition, continuous advances in micro- and nano-fabrication techniques allow the size of mechanical devices to be comparable to the size of some biomolecules, thus resulting in a highly sensitive *mechanical response* and in outstanding *mass resolution* [61–63]. Furthermore, N/MEMS can exhibit extremely high *mechanical compliance*. This enables the measurement of pN forces generated by biological interactions, by translating them into a mechanical displacement, enhancing *force responsivity* [64, 65].

Mechanical biosensors can operate in *static* or *dynamic* mode, depending on whether quasi-static deflection or shifts in the resonance frequency are monitored and thus related to the biological event under study.

4.2.3.1 Static Mode Biosensors

Static-mode biosensors are usually cantilever shaped and typically measure surface stress or surface forces induced by biological entities such as single-base DNA, pathogens or protein biomarkers [66, 67]. Other approaches consider the detection of forces at the tip of cantilevers, using a configuration similar to that of an atomic force microscope (AFM) [68, 69].

Common surface stress biosensors consist of microcantilevers with one active side functionalized to attach a monolayer of receptors that exhibit high affinity to the target molecules, while the opposite passive side is inert. The devices are placed in a fluid cell where the sample solution is delivered. The binding of target molecules to the receptors causes a surface stress change that induces a quasi-static deflection of the cantilever (see Fig. 4.10).

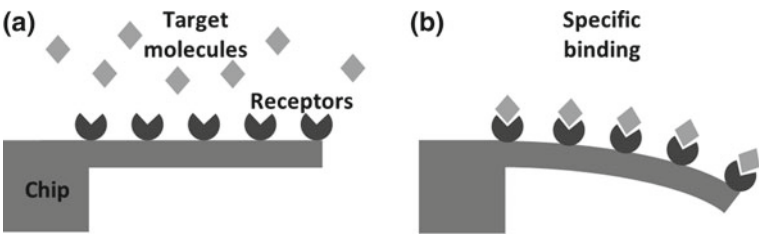

Fig. 4.10 Working principle of a static mode biosensor. Binding of target molecules induces a surface stress, which leads to a quasi-static deflection of the cantilever. This bending can be measured with optical or electrical displacement detection methods

The stress induced cantilever deflection is real time monitored via optical or electrical displacement detection methods. The surface stress variation can be evaluated through the change of curvature the microcantilevers undergo when the sample solution flows over them. According to the Stoney's equation $\Delta\kappa = 6\frac{(1-\nu)}{Eh^2}\Delta\sigma$, where κ is the curvature, ν and E the Posson's ratio and the Young's modulus of the material respectively, h the thickness of the cantilever and $\Delta\sigma$ the surface stress change. The Stoney's equation is only valid under the assumption of plates with unclamped edges. Therefore, in order to take into account the clamped edge of microcantilevers configuration, a correction factor needs to be considered [70, 71].

These devices have shown remarkable label-free capabilities [72], however deflection is highly susceptible to non-specific binding, temperature and flow fluctuations. Very stable flows, together with differential measurements of non-functionalized cantilever help to partially circumvent spurious deflections [67].

4.2.3.2 Dynamic Mode Biosensors

Dynamic mode biosensors are mechanical devices which vibrate close to the resonance frequency of the device f_r proportional to the square root of the ratio between stiffness k and mass m of the structure. An analyte landing or binding on the resonator surface induces a change of its mass (and stiffness [73]), which is transduced into a shift of the resonance frequency, as seen in Fig. 4.11.

Micro- and Nano-mechanical resonators have demonstrated great capabilities in life-science label-free mass sensing applications, such as detection of viruses and single molecules [3, 63, 74]. Mass responsivity is defined as the change in resonance frequency due to a change in mass. $\Re = \frac{\partial f_r}{\partial m} \approx -\frac{1}{2}\frac{f_r}{m}$ [3, 75]. In order to achieve the highest mass responsivity, one can reduce the mass or increase the

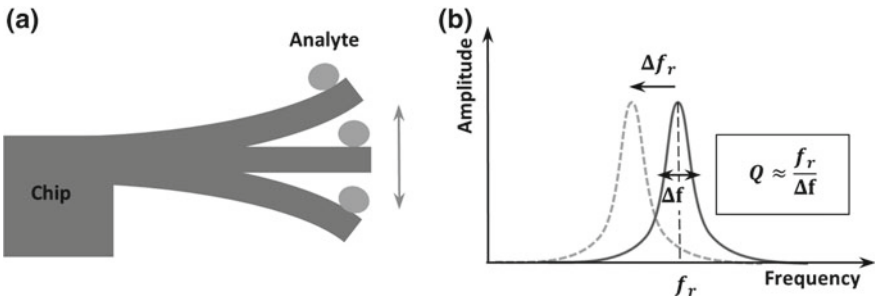

Fig. 4.11 Working principle of a dynamic mode mechanical mass sensor. An analyte landing on the free-end surface of a singly-clamped beam resonator induces a change of its mass and stiffness, which is transduced into a shift of the resonance frequency Δf_r. The accuracy of the measurement of the resonance frequency is defined by the quality factor Q, related to the full width of the half maximum of the resonant peak Δf

frequency (or both). The minimum detectable mass by a mechanical resonator is given by the ratio between the noise and the responsivity, and it is typically given by: $\delta m_{min} \approx \frac{\delta f_{min}}{\Re} = -\frac{1}{2}\frac{\delta f_{min}}{f_r} m$. Using Robbins formula [76], we can then write: $\delta m_{min} \approx -\frac{1}{2} m \frac{1}{Q}\frac{Noise}{Signal}$. Thus, it is clear that a large quality factor, Q, is necessary to optimize the sensing performance. Q determines the slope of the phase versus frequency curve of the device near resonance. It can also be seen as the ration between energy stored and energy lost per cycle of the resonator: $Q = \frac{E_{stored}}{E_{lost}}$.

In order to attain large quality factors, one needs to reduce the energy loss. This typically implies to work in vacuum [66]. However, when tackling real time biosensing applications, like protein or DNA detection, the immersion of the resonator into fluids is inevitable since most biological processes naturally occur in a *fluidic environment*. In this scenario, fluid viscous damping causes a drop of Q of several orders of magnitude.

Detection in Liquids

The main strategies developed to exploit nanomechanical sensor performances for biological detection consist in (i) capture in fluidic phase and detection in vacuum, (ii) measurements in humid environment, and (iii) continuous operations in liquid focused on enhancing the quality factor [66, 67]. The first one will not be detailed here as the operation of the device is not performed in liquid.

Humid environment

Certain biological species like bacteria can grow and survive in humid environment. In this case, even though viscous damping is larger than in vacuum, it does not reach the levels of full immersion in liquid, thus the quality factor remains acceptable. An example of this biodetection is the growth monitoring of Escherichia coli using cantilevers coated with nutritive layers (sugar) and operation in air with 100% humidity [77].

Real-Time monitoring in liquid

There are many other cases, e.g. the detection of analytes, which require full fluidic immersion while the measurement is running. This, as announced before, poses a practical issue since viscous damping degrades Q. The solution for this has been, up to date, limited to a handful of experimental techniques. One example is the use of acoustic modes (QCM and SAW). Another option, considering flexural devices, is to use larger frequencies, higher vibrational modes [78], individual actuation and detection, vertical nanopillars [79–81] and suspended microchannels [82].

Quartz Crystal Microbalance

An interesting device from the performance point of view is the quartz crystal microbalance (QCM). It consists of a quartz disc with electrodes that allow for the excitation of a shear acoustic mode, which has an inherent low viscous interaction with the surrounding fluid (Fig. 4.12) [83]. QCMs are used now in a range of scientific disciplines, such as chemistry, biology, and material sciences, demonstrating also detection of biomolecules and bacteria [84]. The resonance frequencies of these devices are usually in the range of 10–50 MHz. The thickness of the crystal determines its resonant frequency, but at higher frequencies the devices become

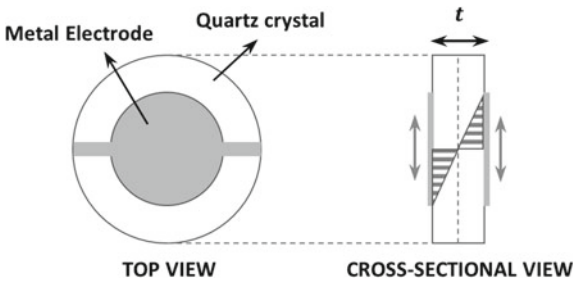

Fig. 4.12 Schematic of Quartz Crystal Microbalance (QCM). A quartz crystal disk oscillates in thickness-shear mode when the metal electrodes deposited on each side of the disk are connected to an alternate voltage signal, generating a bulk shear acoustic wave (BAW)

very thin and too fragile. Because of the device thickness in the range of millimeters, the sensitivity of QCM is limited [84]. The lowest limit of detection of QCM in liquid has been achieved in the work by Cho et al. They demonstrated nanomolar sensitivity for continuous analyte monitoring of C-reactive protein, a biomarker for coronary heart disease, using an indirect-competitive assay [85].

Surface Acoustic Wave Devices

Another example of acoustic sensors are SAW devices, which have been described in the previous paragraph for their capabilities in microfluidic actuation and micro-objects manipulation like mixing, pumping, merging and sorting among other applications [43]. SAW devices have also demonstrated to represent a cost-effective technology for label-free detection of biomolecular interactions, allowing highly sensitive real time detection of biomolecules such as DNA, protein and bacteria [86, 87]. Recently, Senvely and coworkers proposed a low cost innovative system capable of analyzing few picoliters of biological cell samples at high frequencies. Tumor cells are trapped inside microcavities along the SAW device surface. Through interaction with the samples, the resultant SAW reaching the output electrode exhibits a phase delay which is related to the cell mechanical stiffness [88].

SAW devices generate and detect acoustic waves using interdigital transducers (IDT) on the surface of a piezoelectric crystal, typically lithium niobate (LiNbO3) or lithium tantalate ($LiTaO_3$). As shown in Fig. 4.13, an input IDT converts an electrical signal into an acoustic wave through direct piezoelectric effect. On the opposite side, an output IDT converts the acoustic wave back into an electrical signal, through inverse piezoelectric effect. The surface acoustic wave travels along the space between the IDTs, known as the delay-line. The acoustic energy stays confined close to the surface of the PZE crystal in a depth range close to the acoustic wavelength, regardless of the thickness of the complete substrate. For this reason, the wave is potentially very sensitive towards any change on the surface, such as mass loading, viscosity and conductivity changes [86]. To permit the use of a SAW device as a biosensor, analyte-specific molecules are immobilized on the device surface to catch analyte molecules from the sample solution, as shown in Fig. 4.13. Analytes binding to the immobilized receptor molecules will influence the velocity of the SAW and hence the output signal measured by the system electronics [86].

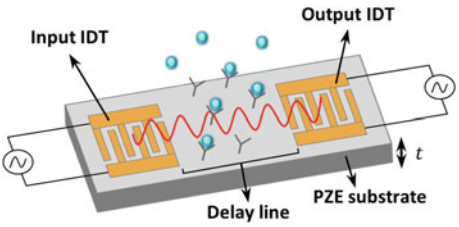

Fig. 4.13 Schematic of a Surface Acoustic Wave sensor (SAW). An input interdigitated electrode (IDT) sitting on a piezoelectric substrate converts an electrical signal into an acoustic wave. An output IDT converts the acoustic wave back into an electrical signal. The surface acoustic wave travels along the space between the IDTs, known as the delay-line. Analyte binding to the immobilized receptors will influence the velocity of the SAW and hence the output signal measured by the system electronics

SAW devices can be found to be as thin as few hundreds of micrometers and their typical frequencies are much larger than those of QCMs. However, the acoustic waves are not purely shear, and thus radiate compression waves into the liquid, which induces larger damping than in the case of shear modes, but lower than in the case of flexural [87].

Suspended Microchannel Resonators

As we have seen above, the minimum detectable mass is proportional to the mass of the device. In order to minimize said parameter, the optimum choice is to work with *flexural devices*, which can reach nanoscale dimensions and masses in the order of picograms, potentially allowing single molecule mass sensitivities. However, flexural devices exhibit out-of-plane vibrations, therefore their energy loss is much larger compared to acoustic resonators.

An important contribute to mechanical biosensing in liquids came from Manalis' group in 2003, when they presented a device inspired to the millimeter scale densitometer developed by Stabinger and co-workers in 1967 [89]. Suspended microchannel resonators (SMRs) are resonant mass sensors for continuous biomolecular detection in a pico-liter fluid volume [82].

SMRs consist of a hollow resonant structure containing embedded microfluidic channels. The fluid to be analyzed flows inside the resonator, thus viscous damping is almost completely suppressed, and mass loading is minimized. Real time analysis of fluidic samples is made possible while the whole device can be kept in dry environment or even in vacuum. SMRs have been successfully employed for several biosensing applications such as measuring single cell mass, density, volume, deformability, viscosity and monitoring cell growth. Quality factors up to 15,000 and very good mass sensitivities down to 1 ag in 1 kHz bandwidth have been demonstrated [90–95]. However, one of the major limitations of resonators with embedded fluidics (SMCs) is the costly and rather challenging fabrication process, with many steps, which include the use of aggressive chemicals.

Two modalities of operation are possible with SMRs devices: flow-through detection and affinity-based capture, shown in Fig. 4.14.

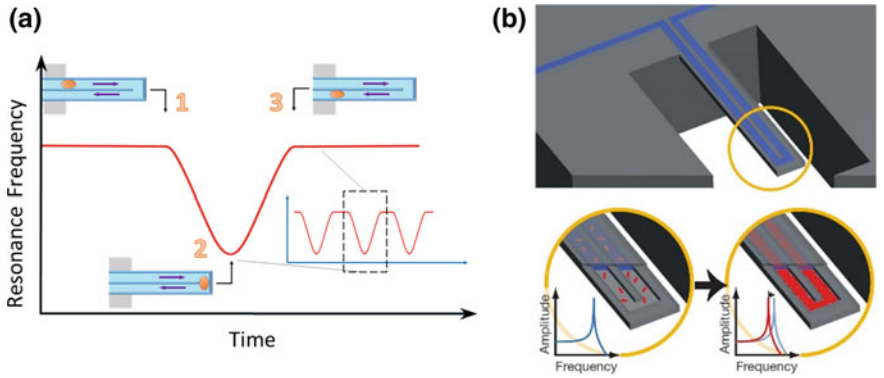

Fig. 4.14 Sensing principle of suspended microchannel resonators. **a** Flow-through detection: a particle flowing inside the embedded microfluidic channel induces a shift in the resonance frequency of the device which is related to the particle mass and position along the structure. **b** Affinity-based capture: target analytes are captured by molecular recognition on a bio-functionalized surface of the device. This induces a shift in the resonance frequency due to mass loading effect [95]

In the *flow-through detection method* a particle travelling inside the microfluidic channel induces a shift in the resonance frequency of the device, which is a function of the position of the particle along the resonating structure, and of the particle density, mass and volume. This approach has been mainly used to study the development of cells along time as a function of different conditions. In this case, the maximum flow rate is determined by the *minimum particle residence time*, which yields sufficient averaging to achieve a detectable signal above the noise floor.

In the *affinity-based capture method* target analytes are immobilized by molecular recognition on the bio-functionalized surface of the microfluidic channel. The functionalization can provide high specificity of capture, reducing false positives that can be caused by particles with similar mass. In this case, the added mass signal from immobilized target analytes can be averaged over a period of time longer than that for free-particle transit through the microchannel. Therefore, in contrast with the flow-through detection method, affinity-capture based SMRs devices are not limited by the analyte minimum residence time. Instead, the sensitivity is determined by the kinetics of diffusion and binding, which can be controlled through geometry and flow-rate.

The main limitation of this type of devices is the throughput, defined as the sample volume that can be analyzed per unit of time [96]. High throughputs can be obtained through pre-concentration of the analyte solution and device parallelization, as recently demonstrated by Cemark and co-workers [91].

4.3 Passive Microfluidics (Magalie Faivre)

4.3.1 Introduction

Microfluidic diagnostic tools provide numerous advantages over conventional macroscale methods in terms of sample volume, low cost, portability and integration in a complete chain of analysis in Lab-On-a-Chip devices. Among the key features of fluidic microsystems is the possibility to structure the geometry at a scale comparable to that of cells, the ability to control precisely the cellular environment and to perform analysis at the single-cell level while dealing with large populations. The high heterogeneity of cell samples, containing many different species at very different abundance levels, is one of the great challenges in clinical research and biomedical engineering. Concentrating, focusing, trapping and sorting these cells are thus critical steps in various biomedical applications including (i) diagnostics, (ii) therapeutics and (iii) cell biology, where the least abundant cells can be the most important. Indeed, some domains such as oncology, stem cells research or infectious disease, have raised great interest in identifying, accumulating and counting various types of "rare cells"—cells present as a very small subpopulation in a large amount of surrounding cells—or bacteria in blood [97]. Rare cells such as Circulating Tumor Cells (CTCs) may be difficult to isolate as large volumes of blood are required to be relevant [98], imposing a very high throughput of the separation technique. For example, HIV diagnostic and theranostic rely on the separation and count of human T-lymphocytes (CD4+) from whole blood [99, 100]. Non-invasive prenatal diagnosis can also be performed by separating rare fetal cells such as Nucleated Red Blood Cells (NRBCs) from peripheral maternal blood [101]. For example, CTCs [102], stem cells [103] and malaria-infected Red Blood Cells (RBCs) [104] would highly benefit from rapid, efficient and low-cost separation microdevices.

Microfluidic cell manipulation and sorting methods can be divided in two: active and passive approaches. Active methods are based on the application of an external field to achieve particle manipulation, (dielectrophoresis, acoustophoresis, magnetophoresis, etc.…) whereas passive techniques rely on the channel geometry and associated hydrodynamic forces to operate on cells. Although it may be considered as a passive sorting approach, the immunological-based separation, which exploits the presence of antibodies at the surface of the cells of interest, will not be discussed here. The different label-free passive techniques rely on several cells intrinsic physical properties such as size, shape, deformability or density to manipulate and sort them. Passive label-free techniques generally require fewest preparation steps than active ones, making it a highly attractive approach for cell manipulation. For detailed information on active techniques, affinity-based methods and their comparison with passive ones, the readers are suggested to refer to specific chapters of the present book or the following review papers from Xuan et al. [105], Bhagat et al. [106], Shields IV et al. [107], Autebert et al. [108] and Gosset et al. [109].

In this section, we aim at introducing and discussing the different approaches available to perform concentration, trapping, manipulation and sorting of cells and their applications. We propose to analyze many passive techniques for cell manipulation, concentration and isolation in microsystems, detailing their mode of action and trying to evaluate their performances to allow comparison. We document potential applications, discuss the main advantages and limitations of the different approaches, and attempt to outline the main remaining challenges in this fast evolving field.

4.3.2 Microfiltration

A commonly employed technique to isolate cells is microfiltration. Most of cell sorting devices using microfiltration rely on both size and deformability to define the pore size and the type of filtration. In the following, we will detail various approaches with one common feature: the use of micropatterns to induce specific behavior of particles flowing in a microfluidic device.

4.3.2.1 Size Exclusion

The use of micropatterns (pillars, weirs, wells, etc.…) is very attractive for size and deformability-based cell sorting or capture. This approach is especially well adapted to the microsystem format where characteristic dimensions are comparable to the typical size of cells. Size-based microfiltration faces many challenges including the heterogeneity of size within a population of cell and membrane clogging. Four types of microfilters have been implemented for whole blood filtration [110]: membrane, weir, pillar and cross-flow (Fig. 4.15a).

Membrane microfilters are composed of well-defined pores, designed to prevent the passage of cells below a critical size. More than 90% recovery of lung cancer cells from spiked blood samples, with a relatively high processing throughput of 10 mL/h, was recently demonstrated using a highly porous polydimethylsiloxane (PDMS) membrane filter-based microdevice [114].

Weir-type microfiltration has been used to produce cell-free blood plasma [115, 116] for diagnostics. The microdevice has been designed such as the sample would flow through a planar groove, small enough to retain all blood cells (Fig. 4.15a). However, very small amount of plasma—typically several tens of nanoliters—was produced due to the use of capillary-driven flow [116]. The obtained filtrate was tested negative for significant levels of hemoglobin and cellular debris.

Pillar-type microfiltration implements micro-obstacles which spacing is chosen adequately to retain cells above a given critical size (Fig. 4.15a). Such design has been successfully applied to the isolation of fetal nucleated RBCs from cord blood using rows of pillars with decreasing spacing [117]. However, it is unsuitable for

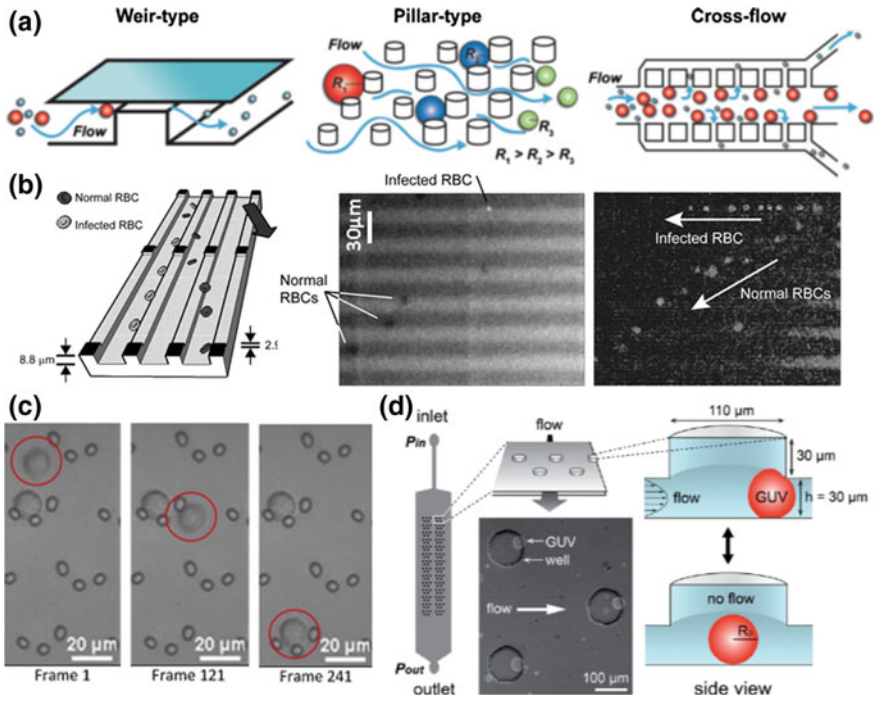

Fig. 4.15 **a** Some examples of implementation of the microfiltration technique: weir-type, pillar-type filters or cross-flow (Reproduced from [109], copyright The Authors (2010) with permission of Springer). **b** Application of the microfiltration to the isolation of malaria-infected RBCs from healthy ones (Reproduced with permission from [111]). **c** The use of crescent-shaped isolation wells has been reported to trap CTCs (Reproduced from [112], copyright (2010) with permission from Elsevier). **d** Example of deformability-based microfluidic device implementing indentations etched in the channel ceiling to trap particles (Reproduced from [113] with permission of The Royal Society of Chemistry)

prenatal diagnosis due to the relatively low throughput achieved (0.35 mL/h) and the high probability of clogging, the cells being trapped in the direction of the flow.

Cross-flow microfiltration was developed to reduce clogging and filter saturation. The working principle is similar, except that the flow is perpendicular to the array of obstacles or weir filter (see Fig. 4.15a). Cross-flow filtration has been used by Sethu et al. to achieve separation of 97% of White Blood Cells (WBCs) from whole blood [118] at a flow rate of 5 µL/min. A similar approach has been implemented by Han et al. [111] to isolate mechanically impaired malaria-infected RBCs, rigidified by the presence of the parasite, from healthy ones. The cells are flown in a channel with several parallel trenches which walls have been dimensioned such as deformable cells can squeeze from one trench to another but stiffer ones cannot. A flow is applied at an angle with respect to the trenches (Fig. 4.15b), allowing deformable healthy RBCs to follow the flow and be collected on one side of the outlet whereas the parasited RBCs keep linear trajectories and are collected on the other side of the

outlet [111]. Reported studies on mechanical filtration microsystems [119] show limited efficiency in the target cell isolation at high throughput. Recent published work reports another approach to overcome clogging: the use of low frequency oscillating flow [120]. They achieve collection of target polystyrene particles with 100% efficiency and demonstrate the separation of CTCs from whole blood (50 fixed MDA-MB-231 cells in 200 μL of blood processed at 200 μL/h).

4.3.2.2 Isolation Wells

Microsytems implementing micropatterns can also be employed to perform cell trapping. Located in the path of the flow, those micropatterns forming cavities are designed such as only one cell gets trapped in it. Such platforms offer the possibility to perfuse different reagents to the individually captured cells and to study their response, which can be highly attractive for drug screening assays in the framework of personalized medicine applications. Di Carlo et al. [121] demonstrate the capture of single HeLa cells using arrays of physical U-shaped hydrodynamic trapping structures. Their microsystem allows both the culture of individual adherent cells and the dynamic control of fluid perfusion with uniform environments. With a similar approach, Tan et al. [112] have demonstrated the capture of CTCs (issued from 8 different types of cancer: breast and gastric carcinomas, tongue and pharynx squamous carcinomas, etc…) in blood using arrays of crescent-shaped isolation wells and their subsequent release for further analysis (Fig. 4.15c). Typically, 100 cells suspended in 1 mL of blood were successfully flown at a pressure of 5 kPa in the device and performances with very low count of cancer cells (typically 1–3 cancer cells in 1 mL of buffer) were evaluated at 81%. Recently, Yamada et al. [113] have reported a clever approach to trap and release giant unilamellar vesicles (GUVs) in a thin and wide microfluidic channel, as they cross indentations etched in the channel ceiling (Fig. 4.15d). The particles being squeezed to flow into the shallow channel, partially relax when entering a well with a larger height, leading to their capture. They demonstrate that GUVs, whose diameter is slightly larger than the channel height, can be trapped and subsequently released by flowing the outer fluid beyond a critical velocity [113]. They report a size-dependency of the critical flow velocity necessary to untrap the GUVs.

In this review we introduced different label-free passive manipulation techniques, which characteristics are gathered for comparison in Table 4.1.

4.3.2.3 Deterministic Lateral Displacement

The implementation of microstructures in a microfluidic device can also be employed to continuously sort cells without clogging. Deterministic lateral displacement (DLD) is a size-sorting technique where cells navigate through an array of posts [122]. Contrary to the previous techniques, there is no retention of cells on the chip as both the cells of interest and the rest of the sample are flowing separately

Table 4.1 Label-free passive microfluidic manipulation and separation techniques

Method	Principle	Properties exploited	Sample	Performances	Flow Rate	Ref.
Microflitration	Size exclusion	Size, deformability	Whole blood*	>97% depletion of WBCs	5 μL/min	[118]
Wells	Cell trapping	Size, deformability	CTCs in PBS[a]	80% CTCs isolation	5 kPa	[112]
DLD[b]	Flow through posts array	Size, deformability, shape	Whole blood	>99% WBCs isolation	0.3 nL/s	[122]
Hydrophoresis	Flow alterations	Size, deformability, density	~2% hematocrit blood	210-fold enrichment of WBCs	1 μL/min	[123]
Gravity	Cell sedimentation	Size, density	3 and 20 μm bead suspension	~100% isolation of 2 populations	1.2 mL/hr	[124]
Hydrodynamic filtration	Streamline modification	Size, shape	Liver cells	~100% hepatocytes isolation	50 μL / min	[125]
PFF[c]	Streamline modification	Size	0.13% hematocrit blood	80% RBCs isolation	20 μL/hr	[126]
Inertia in straight channels	Lift forces	Size	E. coli in diluted blood	300-fold enrichment of bacteria	18 μL/min	[127]
Inertia in curved channels	Lift and Dean drag forces	Size	Beads suspension	Sorting rate of 1 g/hr	1.5 mL/min	[128]
Fahraeus effect	Hydrodynamic focusing	Size, deformability	16% hematocrit blood	24% plasma recovery	200 μL/hr	[129]
Leukocyte margination	Steric margination	Size, deformability	Whole blood	94% NCs[d] isolation	5 nL/s	[130]
Bifurcation law	Hydrodynamic force	Size, deformability	Whole blood	25% volume of plasma isolated	4 μL/min	[131]

*Whole blood corresponds to 45% hematocrit

[a]PBS: Phosphate Buffer Saline, [b]DLD: Deterministic Lateral Displacement, [c]PFF: Pinch Flow Fractionation, [d]NCs: Nucleated Cells

out of the system. At low Reynolds number, an object entering a streamline will tend to follow it, thus having a deterministic behavior. When encountering an obstacle, the behavior will change according to the particle size. Indeed, if the particle has a typical size smaller than a critical hydrodynamic diameter D_c, it will follow the main stream line, circumventing the obstacle. In the contrary, if the object size is larger than D_c, the object will bump into the obstacle which will lead to a shift in stream line (Fig. 4.16a). The critical hydrodynamic diameter D_c is related to the inter-posts distance d and the period of the array N according to the following equation [132]:

$$D_c = \sqrt{\frac{N}{3}}.\frac{d}{N}, \tag{4.1}$$

The influence of the geometrical parameters on D_c was carefully evaluated by Inglis et al. [135] and have been used to fractionate undiluted whole blood samples [122], separate parasites from human blood [136] and isolate cancer cells [137]. By tuning the posts size, their spacing, as well as the shift between adjacent post rows, Huang et al. [138] demonstrated that D_c could be tuned precisely enough to sort 0.8, 0.9 and 1.03 μm in diameter particles upon their size. Obstacles can be any shape: cylindrical, rectangular or triangular [127]. Tottori et al. [139] used a DLD microfluidic device to sort viable Jurkat cells from nonviable apoptotic ones, the latter being smaller due to shrinkage and fragmentation. However, such microsystem is much more complicated than it seems as one need to take into account the deformability of the cells. Actually, DLD is a size-based separation technique but it is also sensitive to shape (Fig. 4.16b) and rigidity (Fig. 4.16c) of the target cell as shown by Beech et al. [133] on RBCs. Finally, thermally tunable DLD has been demonstrated [134] recently. Indeed, by implementing poly-N-isopropylacrylamide (poly-NIPAM)—a thermo-sensitive hydrogel known to be swollen or shrinked, respectively below and above a critical temperature—pillar arrays, it is possible to tune at will the size and spacing of the posts, by adapting the temperature as illustrated Fig. 4.16d.

4.3.3 Hydrophoresis

The introduction of micropatterns in the microfluidic channel can finally be exploited to perform cell focusing using a phenomenon referred to as hydrophoresis. This technique relies on the formation of a lateral pressure gradient within a microfluidic channel due to the presence of an array of slanted obstacles on the microchannel floor and/or ceiling; the apparition of associated micro-vortices altering the flow [140] and leading to the focalization of particles (Fig. 4.17a). Using this phenomenon, Choi et al. have developed a device that exploits differences in both the size and deformability of cells for passive sorting [123]. This principle was used to demonstrate a 210-fold enrichment of WBCs from RBCs with

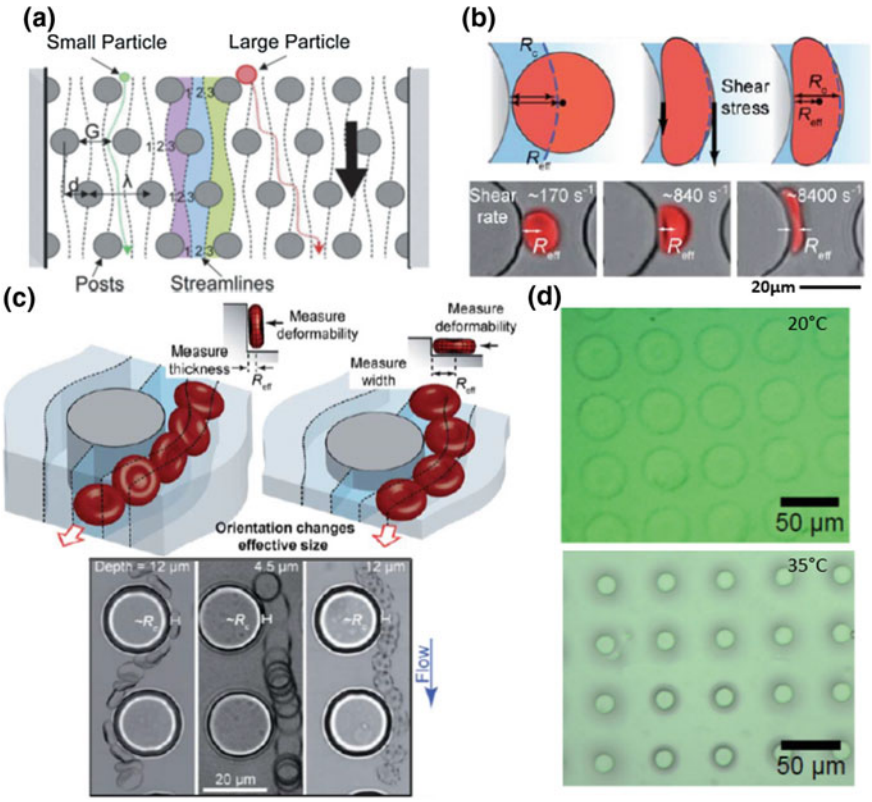

Fig. 4.16 **a** Deterministic lateral displacement approach is a size-based separation method relying on the posts size, the distance between them, as well as the relative shift be bigger ones are deflected on one side of the device (Reproduced from [122], copyright (2006) National Academy of Sciences, U.S.A.). DLD have also been demonstrated to be sensitive to cell **b** shape and **c** rigidity (Reproduced from [133] with permission of The Royal Society of Chemistry). **d** poly-NIPAM pillar arrays allow thermally tunable DLD (Reproduced from [134] with permission from Chemical and Biological Microsystems Society)

a throughput of 4×10^3 cells/s. More recently, the same group has reported the recovery of 98.5% of CTCs spiked in blood (1 MCF-7: 7500 blood cells) at a flow rate of 44 μL/min [141].

Similarly, a device with successive ridges along the channel ceiling has been shown to focus and sort cells [143, 144]. This microsystem contains an array of herringbone shaped slanted grooves in the ceiling of a microfluidic channel that passively focuses cells to specific location of the channel upon their density, thus acting their separation. They successfully sort a mixture of two bead populations whose density difference is as small as 0.1 g/cm^3. With a different design, Sollier et al. [142] present a ridgeless microvortex, introducing a sudden geometrical

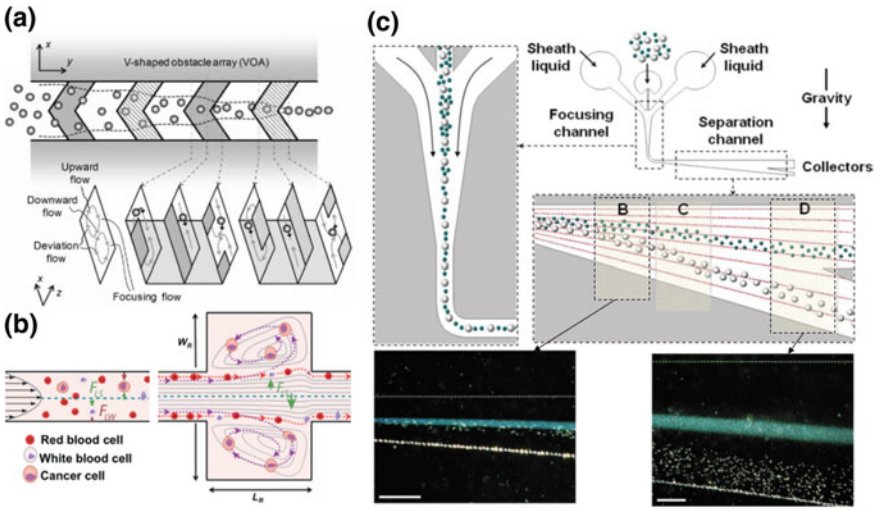

Fig. 4.17 **a** Hydrophoresis manipulation techniques include ridge-based microvortex (Reproduced with permission from [140] Copyright (2008) American Chemical Society) and **b** microvortex using a sudden geometric expansion (Reprinted from [142] with permission of The Royal Society of Chemistry). **c** Size-based particle sorting has been demonstrated using a gravitational force with hydrodynamic amplification (Reproduced with permission from [124], copyright (2007) American Chemical Society)

expansion in a microfluidic channel to create predictable recirculations to capture CTCs from blood as illustrated on Fig. 4.17b.

4.3.4 Gravity

Huh et al. [124] have demonstrated the size-based particle sorting using gravity with hydrodynamic amplification. Briefly, the randomly distributed particle suspension is injected and tightly focused in one dimension by sheath flows into the device parallel to gravity. After flowing around a 90° turn, the stream of particles flows in a divergent channel normal to gravity and are allowed to sediment at a speed depending on their size, their density relative to that of the suspending fluid and the external viscosity (Fig. 4.17c). Sorting of objects with different size is amplified by the asymmetrical geometry of the widening, creating a downward-angled flow. This sedimentation-based microsystem has been successfully demonstrated with polystyrene particles and polydispersed droplets, with typical flow rates of 1 mL/h. However this technique has only been demonstrated with the separation of objects with very large size difference and waits to be applied to cell sorting. Gravity is also employed in centrifugal microfluidic where

microsystems developed on disc, also known as Lab-On-a-Disc, are spinned in order to both move the fluid inside the chip and perform separation [145].

4.3.5 Hydrodynamics

Several techniques will be discussed in the next section due to their similarities in terms of operating principles. These label-free passive manipulation techniques rely on the behavior of particles in a laminar flow, at low Reynolds number, where the center of mass of the particle follow the associated fluid streamline.

4.3.5.1 Hydrodynamic Microfluidic Filtration

Hydrodynamic filtration was introduced by Yamada et al. [146] for size-based separation in a microfluidic device. In this technique the sample is injected in a main channel having multiple side branches. Small amount of liquid is repeatedly drained through the side branches, hence concentrating and aligning all the cells along the sidewalls of the main microchannel (Fig. 4.18a). The size difference positions small particles closer to the sidewall than larger ones, allowing the former to be filtered out earlier. The size threshold is determined by the relative flow rate in the main and side channels, which depend on the flow resistance of each branch and may be adjusted by changing the pressure drop applied to each channel. Yamada et al. applied this technique to the selective enrichment of leukocytes from 10-folds diluted blood at 20 μL/min [146] and liver cells in culture medium at $\sim 2 - 3 \times 10^6$ cells/mL at 50 μL/min with a throughput higher than 2×10^5 cells/min [125]. Recently Aoki et al. [147] applied the principle of hydrodynamic filtration to the focusing of 5 μm particles along the centerline of a main microchannel. They used multiple loop side channels to drain the liquid out upstream, before re-injecting it into the main channel from both sides simultaneously, serving as sheath flow to focus the particles.

4.3.5.2 Pinched Flow Fractionation

Pinched flow fractionation (PFF) is a label-free hydrodynamic technique for size-based separation introduced by Yamada et al. [148]. This method relies on the use of a sheath buffer injected such that the particulate content of the sample is pushed against one wall in a pinched segment of the channel. Due to the difference in size, the center of mass of small cells are located on streamlines closer to the wall than that of bigger ones. This difference in lateral position is significantly amplified by the parabolic velocity profile in Poiseuille flow. As the channel widens after the pinched segment, the particles of different size are rapidly dispersed perpendicular to the main flow, allowing them to be collected into distinct outlets (Fig. 4.18b). Unless

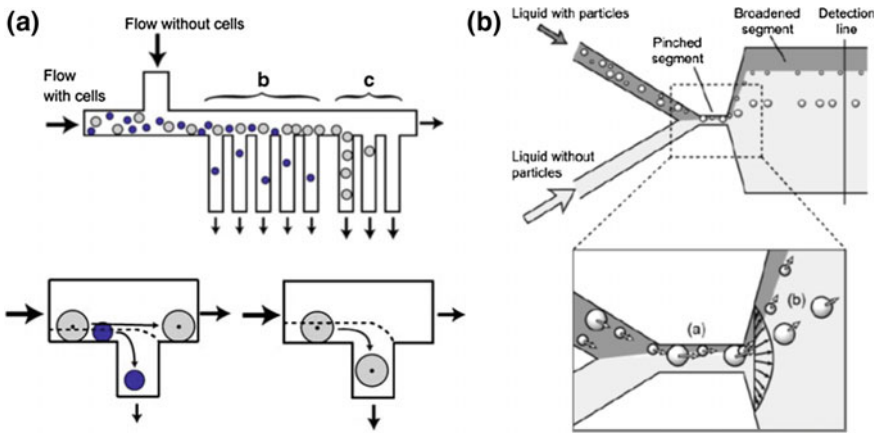

Fig. 4.18 **a** Hydrodynamics filtration (Reproduced from [125], copyright Springer Science + Business Media, LLC (2007) with permission of Springer) and **b** Pinched flow fractionation (Reproduced from [148], copyright (2004) with permission of Springer) are hydrodynamics techniques exploiting the difference in position of the particles center of mass relative to the channel wall according to their size

other separation techniques relying on the device geometry (size and spacing of microstructures, radius of curvature of the channel, shape of micropatterns…), cells of varying sizes can be separated effectively in the same device by adjusting the flow rates of the sample and sheath buffer. Takagi et al. [126] have improved the separation efficiency by playing with the hydrodynamic resistance of the different outlets. They have shown enrichment of RBCs from a 0.3% diluted blood suspension, at a flow rate of 20 μL/h, with a separation efficiency above 90% [126]. Higher flow rates are usually avoided as inertial forces acting on the particles tend to affect their motion, and thus the sorting efficiency. Recently Lu et al. [149, 150] have demonstrated a continuous shape-based separation of spherical and peanut-shaped rigid particles of equivalent spherical diameters. This technique, referred to as elasto-inertial pinched flow fractionation, exploits the dependence of the lift on the shape of a particle suspended in viscoelastic fluids, to amplify the separation induced by the pinched flow fractionation microdevice [149].

4.3.6 Inertial Forces

In microchannels, inertia is usually neglected as flow is considered laminar in absence of turbulence (i.e. for Reynolds number Re above 2000). However, for Re typically ranging from 1 to 100, inertial effects can become significant and perturb the particles trajectories, which no longer follow streamlines. These inertial forces can therefore be exploited to precisely manipulate the cell position within these

systems. For example, in a circular pipe, initially randomly distributed particles tend to concentrate at an equilibrium position corresponding to 0.6 times the pipe radius [151]. The number and location of the particles equilibrium positions may be tuned by controlling the channel geometry [128, 152]. For more detailed explanations, an interesting review by Di Carlo highlights the physics and the applications of this technique toward high-throughput cell separation [153].

4.3.6.1 Inertial Forces in Straight Channels

Lateral deviation of cells—away from the walls—in a straight microchannel occurs because of the competition between two inertial lift forces: the shear-induced and the wall-induced lift forces [154]. As a result, particles will move to specific equilibrium positions within the channel cross-section, according to their size (Fig. 4.19a). Di Carlo et al. were among the first to investigate the inertial focusing of objects in straight microchannels [128]. They observed that initially uniformly distributed microbeads of 9 μm in diameter were focused along the centers of each of the four walls (see Fig. 4.19b) as the Reynolds number was increased (Re = 90), leading to local particle concentration. Using this principle, Bhagat et al. have demonstrated continuous filtration of particles from a suspension [155]. The same phenomenon has been implemented in microsystem in order to achieve controlled encapsulation of single cells into microdroplets [156] and sheathless focusing of cells for high throughput flow cytometry [157].

Recently, Di Carlo's group [158] studied inertial focusing of particles in non-rectangular cross-section channels, such as semi-circular or triangular shapes. They demonstrated that they can modulate the location and number of focusing positions depending on the cross-section shapes and Reynolds number. By connecting channels with different cross-sectional shapes, they reported the focusing of microparticles to a single stream with 99% purity [158].

4.3.6.2 Inertial Forces in Curved Channels

In a curved channel, the curvature induces an additional force referred to as the Dean drag force. Indeed higher momentum fluid at the center of the channel moves lower momentum fluid near the walls, resulting in two counter-rotating vortices—referred to as the Dean vortices—normal to the main flow [159]. The Dean drag force will concentrate particles on specific flow lines at the expense of others. Di Carlo et al. [128] observed that the four equilibrium positions observed in straight channels, were reduced to two in a symmetric sinusoidal channel and to a single equilibrium position in an asymmetric channel (Fig. 4.19b). They demonstrated that cells could be differentially focused and sorted based on size under laminar flow, with a high throughput (1.5 mL/min), using a serpentine pattern (Fig. 4.19c). Later, the same group demonstrated the focusing and sorting of cells using a spiral channel [160]. Wu et al. demonstrated the isolation of bacteria from diluted blood with a

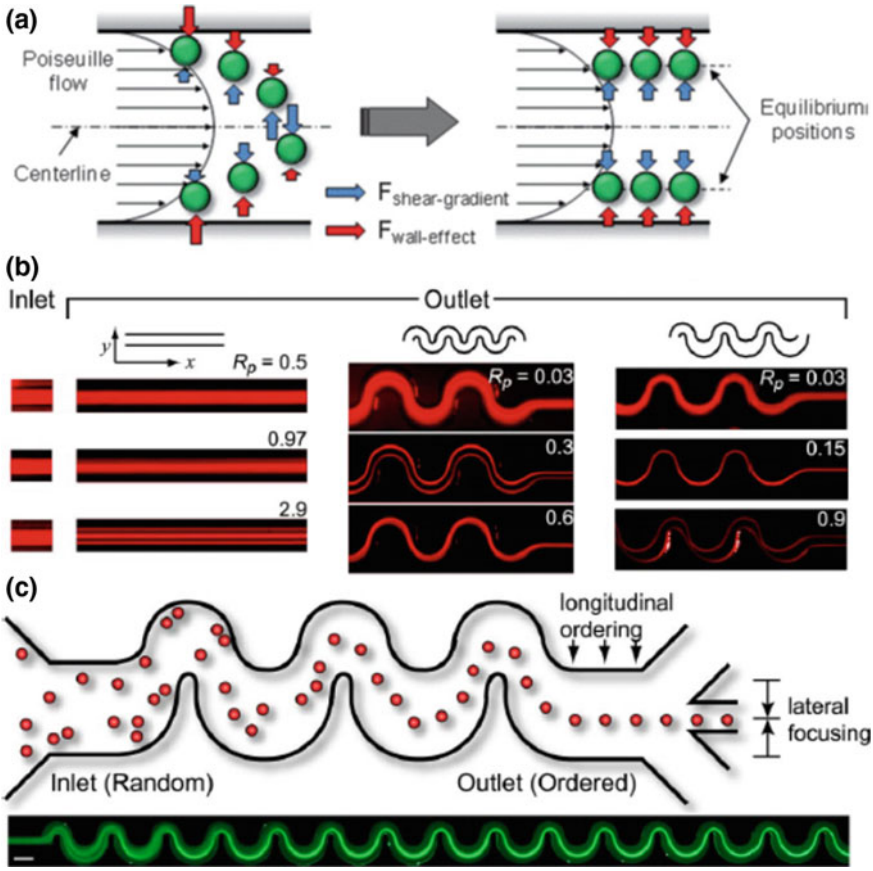

Fig. 4.19 **a** Inertial forces can be exploited to manipulate the cell position within the channel (reproduced from [154] with permission of The Royal Society of Chemistry). **b** In a straight channel, particles tend to be focused along the centers of each of the four walls, whereas in a curved channel, the number of equilibrium positions is reduced to two. **c** Di Carlo's group demonstrated the focusing of particles using an asymmetric sinusoidal channel. R_p represents the Reynolds number associated with the particle and includes parameters describing both the particle and the channel through which it is translating. (Reproduced with permission from [128], copyright (2007) National Academy of Sciences, USA)

purity above 99% and a recovery rate of 62%, at a flow rate of 15 μL/min [127]. Dean Flow was used to separate two types of neuronal cells with average diameters of 8 and 15 μm respectively, with an efficiency of 80% and a throughput of the order of 10^6 cells/min [161]. More recently, Bhagat et al. managed to isolate 90% of tumor cells in a 20% hematocrit blood sample spiked with MCF7 breast cancer cells, at 4 mL/h maximum flow rate [162]. The use of a spiral channel presenting a trapezoidal cross section has been demonstrated to further improve the performance of such device to focus and separate cells [163, 164].

Finally, as inertia-based focusing methods exploit the particularities of flow at high flow rate (i.e. large Re), it may offer a high throughput, which makes it suitable for high-speed applications such as flow cytometry. On the other hand, this technique may be limited to only dilute samples, the efficiency being deteriorated by cell-cell interactions.

4.3.7 Biomimetic

The concept of biomimetic techniques for cell manipulation consists in biologically inspired designs exploiting cell behavior observed in vivo, most of the time in blood vessels.

4.3.7.1 Fahraeus Effect

One of the most famous hemodynamic phenomenon of the microcirculation is the Fahraeus effect [165, 166]. For instance, in veins with a diameter smaller than 300 μm, RBCs tend to drift away from the high shear regions adjacent to the vessel wall, resulting in their accumulation at the center of the blood vessel. Thus leaving a "cell-free" plasma layer adjacent to the vessel wall [167]. Faivre et al. [129] used a geometric constriction to enhance the size of the "cell-free" layer (Fig. 4.20a). They report the recovery of 24% of the initial blood plasma from a 16% hematocrit blood suspension (dilution 1:3), at a working flow rate of 200 μL/h [129]. Key parameters of this approach include the sample viscosity—which can be tuned by dilution—the flow rate, the cells volume and deformability, as well as the shape and size of the geometric constriction. Later, Sollier et al. [168] has improved the performances of such devices by adding geometrical singularities such as ear-cavities or corner-edges. They reached a recovery of 10.7% of the plasma, at a flow rate of 100 μL/min, from a blood sample diluted at 1:20. The extracted plasma presented a purity similar to that of centrifugation methods [168].

4.3.7.2 Leukocyte Margination

As the large number of RBCs migrate towards the center of the blood vessel, mechanical collisions between RBCs and WBCs—much larger and stiffer than RBCs—displace the leucocytes near the walls. This phenomen is referred to as the leukocyte margination. Shevkoplyas et al. [169] demonstrated the possibility to sort WBCs from blood by exploiting leukocyte margination. Briefly, whole blood is flown through multiple symmetric and asymmetric bifurcations (Fig. 4.20b). Most of the RBCs flown in the wider outlet, while marginalized leukocytes entered the narrower outlet, leading to nearly 10-fold enrichment of WBCs. Jaggi et al. [172] increased the throughput (in the range of μL/min) by using higher microchannels.

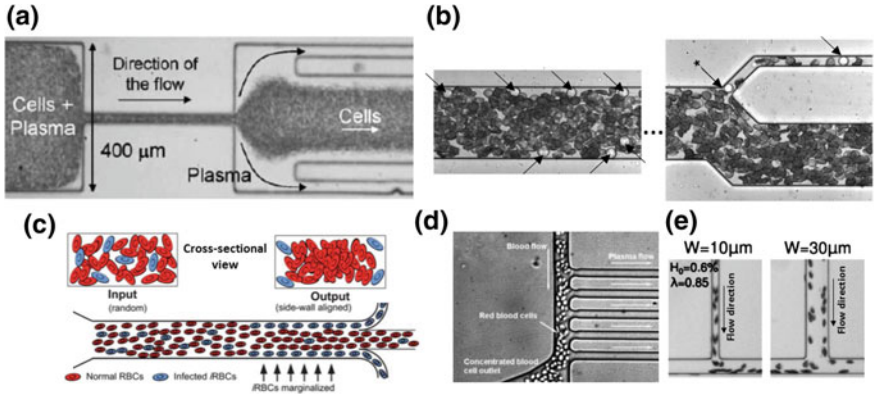

Fig. 4.20 Biomometic approaches include **a** the Fahraeus effect (Reprinted from [129], copyright (2006), with permission from IOS Press), **b** the leukocyte margination (Reprinted with permission from [169], copyright (2005) American Chemical Society) which has also been applied to the isolation of **c** mechanically impaired malaria-infected RBCs (Reproduced from [170] with permission of the Royal Society of Chemistry), **d** the bifurcation law (Reproduced from [131] with permission of the Royal Society of Chemistry) and **e** its inverse in the case of very low hematocrit (Reprinted from [171], copyright (2016), with permission from Elsevier)

Recently, Hou et al. [170] took advantage of the greater rigidity of malaria-infected RBCs (iRBCs) to perform separation of parasited cells in microsystem based on the same principle as illustrated Fig. 4.20c. They claim nearly 75% of separation efficiency for early stage iRBCs, where deformability is only slightly altered compare to healthy RBCs, and more than 90% for late stage iRBCs, with flow rates of 5 µL/min.

Finally, an automated biomimetic microfluidic device made for sorting nucleated cells population from unprocessed whole blood sample was presented [130]. This device is composed of successive triangular channel expansions that mimic the post-capillaries venules expansions in human body. The authors report an extraction of 90% of the nucleated cells with 45-fold enrichment in concentration, at the rate of 5 nL/s [130]. The physics underlying the leukocyte margination, i.e. the "crowding" effect of RBCs on WBCs, favors high RBCs concentration. This technique is thus compatible with the use of whole blood samples, hence avoiding additional sample preparation steps.

4.3.7.3 Bifurcation Law

When a microchannel splits into two channels, a particle will follow different streamlines according to its initial position. In the case of a bifurcation, the flow velocity difference between the two branches decides of the particle trajectory. For example, RBCs flowing at a microchannel split will predominantly choose the daughter channel with the higher flow rate. This effect is referred to as the

Zweifach-Fung effect—also known as the bifurcation law—and has been exploited by Yang et al. [131] in a microsystem to achieve plasma extraction from a blood sample (Fig. 4.20d). Very recently, Shen et al. [171] shown that the inverse of the Zweifach-Fung effect can occur if the hematocrit is small enough. Indeed, in such conditions, they observed that RBCs flow preferentially in the daughter channel with the lower flow rate (Fig. 4.20e), leading to hematocrit in that branch even greater than in the parent vessel [171]. They explain this result by a complex organization of the RBCs prior to the bifurcation and they highlight the extreme dependence of RBCs transport on channel geometry and cell mechanical properties.

4.3.8 Conclusion

In this review we introduced different label-free passive manipulation techniques, which characteristics are gathered for comparison in Table 4.1.

Here the term passive refers to microfluidic devices relying predominantly on channel geometry and/or associated hydrodynamic forces, whereas active describes microsystems using an external force field to function. We chose not to discuss here immunological techniques, where antibody-antigen associations are exploited to achieve cell capture, separation or labelling. The extensive literature in the field underlines the strong interest drawn by label-free passive techniques to manipulate, concentrate, trap, isolate or sort cells using these approaches. Many of the methods presented are at the proof-of-concept stage and few have demonstrated their performances on actual clinical samples. Although they present the advantage on active techniques to be easily manufacturable and to provide cells with minimum residence time under harmful conditions, they still need to overcome some limitations such as low selectivity and low throughput. Advances on parallelization and other scale-up approaches are required especially when rare cells (e.g. CTCs in blood) are involved, as CTCs levels can be as low as 1 cell/mL in early stages. Another drawback of these techniques relying on microscale fluid dynamics, is the need to integrate precise and autonomous flow handling solutions. Finally, the sample preparation procedure often associated may impact the performances of the manipulation due to user variations. Therefore building a microfluidic device that require minimal sample preparation and reducing the dimensions of the apparatus associated with the chip remains a major challenge to be commercially viable.

The selection of the adapted method will depend on the properties of the target cells regarding those of the rest of the sample, and on the needs of the application (efficiency, reliability, simplicity, throughput…). Current microfluidics technology has already demonstrated that it can be used to separate and analyze diseased or rare cells from a sample, more rapidly, with more sensitivity and in a more controlled way. Ultimately, the goal is to develop a portable diagnostic tool—the so-called Lab-On-a-Chip—integrating a whole chain of complex processes needed to perform the desired analysis. Such devices will have tremendous applications in cell biology research, diagnosis, drug screening and personalized medicine.

4.4 Mechanics for Biodevices

4.4.1 Introduction

Biological cell mechanical properties are mainly dictated by the characteristics of its cytoskeleton, which is an elaborate network of polymer fibers [173]. One of the primary applications of the mechanical phenotyping is the identification of pathological cells. Indeed various pathologies and modifications of cell states are reported to influence cell mechanical properties. For example, variation of Red Blood Cells (RBCs or erythrocytes) deformability is associated with malaria [174] and sickle cell anemia [175], White Blood Cells (WBCs) deformability varies in sepsis [176] and acute respiratory distress syndrome [177], and increase deformability of metastatic cancer cells [178] and drop of stiffness during stem cell differentiation [179] have been observed. A better understanding of cell deformability and its interactions with physical environment may imply enormous developments in disease diagnostics, therapeutics and drug screening assays. Although conventional techniques allowing the quantification of cellular mechanical properties, such as atomic force microscopy (AFM), micropipette aspiration and optical tweezers [180] are well-established, they require sophisticated equipments and skilled personal and most importantly are low throughput (of the order of several tens of cells per day). Due to a match between cellular length scales and typical sizes accessible by microfabrication methods, microfluidic technologies propose attractive engineered microenvironments for the study of cellular mechanics compatible with high throughput. The present review begins with an overview of the sub-cellular organization contributing to overall deformability and mechanical response of cells. We then describe recent advances in microfluidic assays for single cell biomechanical characterization. Finally, limitations of current systems and ways in which they can be improved are discussed.

4.4.2 Biomechanics of Cells

Cell mechanical behavior is inextricably related to their intra-cellular composition and architecture, particularly the cytoskeleton. The cytoskeleton is a complex 3D network of biopolymers which primarily defines cell shape and mechanical response to physical stresses and plays a central role in mechanotransduction, mitosis and migration [173]. It is mainly composed of actin microfilaments, intermediate filaments and microtubules. Actin microfilaments are linear polymers that prevent overall cell deformation in response to external stimuli and can polymerize into helicoidal filaments and depolimerize within minutes to facilitate cell motion. Intermediate filaments form an intracellular intricated network connecting the nucleus to the plasma membrane and other organelles. They provide cell structural integrity and resist tension at strain levels where actin networks do not

retain their structural integrity [180]. Microtubules consist in tubulin polymers that contribute to the transport of intra-cellular components within the cell and resist compression. Both the composition and the organization of these combined elements contribute to the cell mechanical phenotype [173]. The interaction of a cell with its environment can also dramatically influence its mechanical properties. Indeed when spread on a surface, adherent cells exhibit a different cytoskeleton conformation than when in suspension, leading to differences in mechanical response to solicitations [181]. In the case of adherent cells, the polymerization/depolymerization of cytoskeleton components in response to both intracellular and extracellular stimuli may significantly alter the global cell mechanical signature. This is especially noticeable during biological processes such as cell division, or cell-cell contacts where extensive cytoskeletal remodeling occurs.

The cell membrane contributes also to the cell mechanical properties due to its connections to the cytoskeleton. It passes strains and stresses on the intracellular tensile and compressive components. For small deformations, membrane viscoelasticity can contribute to overall cell mechanical behavior. It is especially relevant when cells are in suspension, which is the case in flow-based approaches, where viscoelastic characteristics of the membrane plays a role in the cell distribution within the channel [182] (see Sect. 4.3). The presence of the nucleus and other organelles can contribute locally to the mechanical properties of the cell according to their physical size. High-resolution mechanical mapping of flattened cells using AFM presents different rigidity, depending if the measurement has been performed over the nucleus or over cytoplasmic and cytoskeletal areas [183].

The RBC membrane possesses a unique structure responsible of their remarkable mechanical properties (deformability, elasticity, shear resistance, etc.…) allowing them to go through the small capillaries of the microcirculation. RBCs have an elastic 2D mesh-like spectrin cytoskeleton anchored to the internal side of a lipid bilayer [184]. The membrane of the erythrocyte encloses a cytoplasm made of hemoglobin—allowing the transportation of oxygen through the organism—which viscosity at 25 °C is 10 mPa.s. Together with the cytoplasmic fluid and the absence of nucleus and other organelles, the membrane controls the overall deformability of the cell. Under normal conditions, the membrane deforms at constant area and exhibits both elastic and viscous behaviors. The extension of the membrane is governed by the lipid bilayer, which tends to resist area expansion. The shear resistance of the membrane is directly linked to the density of spectrin and thus, to the cytoskeleton [185]. RBCs have been extensively studied in the past fifty years in order to characterize mechanical phenotypes associated with both healthy and pathological states.

4.4.3 Microfluidic Mechanical Characterization of Cells

A wide variety of experimental biophysical assays have been used to probe deformability of living cells. For example AFM and other indentation techniques

allow monitoring the cell deformation in response to a force applied through physical compression or indentation of a probe and can be used to extract cell elastic and viscoelastic properties. In micropipette aspiration, either a portion or a whole cell is aspired into the opening of a micropipette while monitoring the extension of the membrane, leading to the evaluation of the viscoelastic properties locally or at the whole-cell level, respectively. Unlike AFM and micropipette aspiration, optical tweezers are attractive mechanical assays because they do not necessarily require mechanical contact with the target cells. Optical tweezers uses a highly focused laser beam to create a 3D light gradient exerting a force on the cell, relying on the dielectric contrast with the surrounding media. Although these conventional techniques are well-established, they are extremely low throughput (several tens of cells per day typically), which makes it unadapted to diagnostics and biomedical applications, where millions of cells per tens of minutes need to be processed. This section highlights emerging microfluidic techniques addressing this throughput challenge.

4.4.3.1 Optical Stretcher

A microfluidic version of the optical tweezers has been developed by Guck et al. [186] and is referred to as optical strecher. It consists in a two-beam laser trap optimized to serially deform isolated cells flowing through a microfluidic channel (Fig. 4.21a). The cells are being individually stretched at forces on the order of 200–500 pN, which is still not sufficient to induce large deformation. They found that deformability, probed using optical forces, is sensitive enough to detect changes between non-malignant (MCF-10), cancerous (MFC-7) and even metastatic (modMCF-7) human breast epithelial cells [186]. Mechanical phenotyping of cells without any modifications or contact was demonstrated with relatively high throughput (1 cell/min) despite the fact that we are still far from the intended throughput. The same group demonstrated the measurement of the elasticity of malaria infected RBCs (iRBCs) using the optical stretcher [187]. The device combines the selectivity and sensitivity of single-cell elasticity measurements with a throughput that is higher than conventional single-cell techniques. One drawback of this technique is the exposure of cells to the laser beam during stretching.

4.4.3.2 Electro-Deformation

Transient deformation of cells in a high-frequency electric field (Fig. 4.21b) is reported to allow quantitative measurements of the shear elastic modulus and viscosity of plasma membranes of healthy RBCs (hRBCs) [188]. It relies on the principles detailed in Chap. 6. Using analytical models or numerical simulations, estimation of healthy RBCs (hRBCs) shear modulus $\mu = 6.1 \times 10^{-6}$ N/m and membrane viscosity $\eta_m = 3.4 \times 10^{-7}$ N $\cdot$ s/m are obtained and present a good agreement with the micropipette results of Evans et al. [190]. Electro-deformation

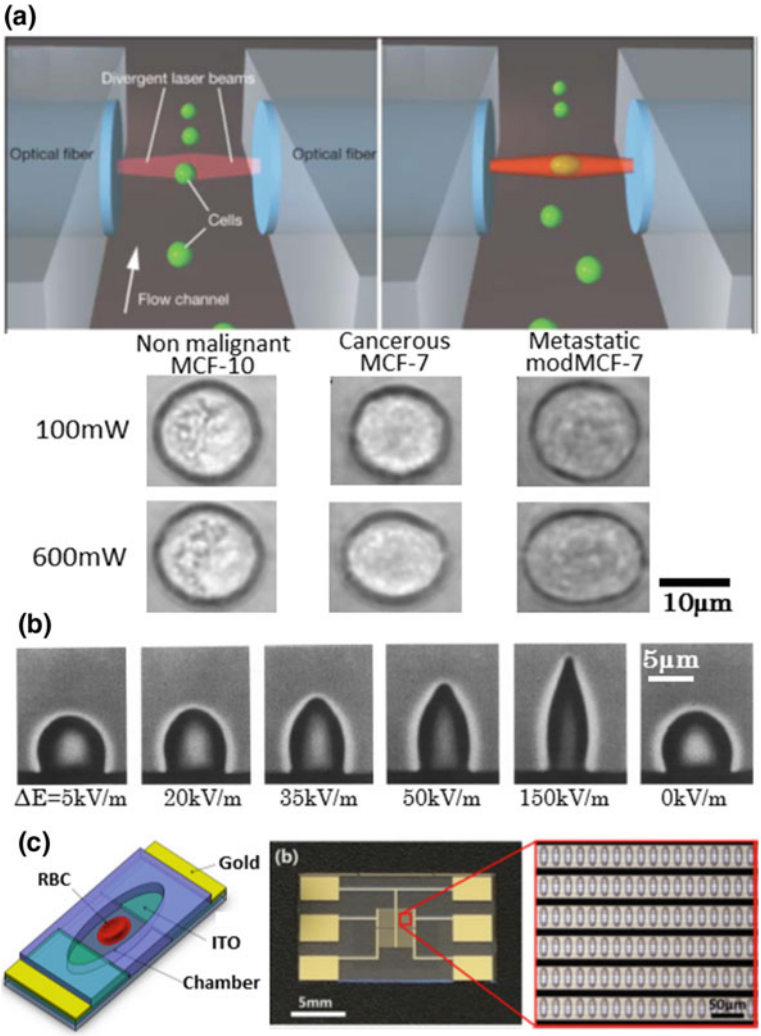

Fig. 4.21 **a** Principle of the optical stretcher developed by Guck et al. Flowing cells get stretched when intercepting the laser beam. Correlation between elongation and metastatic characteristic of breast cell lines has been observed. (Reproduced from [186], copyright (2005) by the Biophysical society, with permission from Elsevier). **b** Electro-deformation of a RBC; cell elongation increases with the applied electric field (reproduced from [188], with permission from Elsevier). **c** Schematic view and actual pictures of the single-cell microchamber array chip allowing mechanical characterization with improved throughput (Reproduced from [189] with the permission of AIP Publishing)

has also been used to quantify the deformability of individual eukaryotic cells [191, 192]. Recently, in order to improve the throughput, a single-cell microchamber array chip was proposed to trap and deform individual RBCs [189] (Fig. 4.21c). One drawback of electro-deformation is the necessity to suspend the cells in a buffer of low conductivity, which add sample preparation steps prior to analysis and lead to rapid aging of the cells [188].

4.4.3.3 Compression Experiments

The discrimination of two different cell types (neutrophiles and fibroblasts) known to have different cytoskeletal structures has been reported using microfluidic compression experiments [193]. The method relies on the observation of the deformation resultant of the cell compression by an actuated flexible membrane (Fig. 4.22a). The relaxation time—the characteristic time necessary for the cells to recover their equilibrium shape as compression is stopped—is used to discriminate two cell lines. Changes in the mechanical response due to disruption of the cellular actin network using Cytochalasin D—an inhibitor of actin polymerization—is also highlighted [193]. With a similar approach, Kim et al. [194] used difference in the bulge generation associated with cell compression, to identify cancerous (MCF-7) from non-malignant breast cells (MCF-10A). Indeed upon cell compression by a flexible membrane and beyond a given strain, cellular membrane expands and small bulges form on the peripheral cell membrane. They explain these bulge formations where cytoskeleton detaches from the membrane bilayer, by a lower amount of actin present in cancerous cells than in normal ones [194].

Compression experiments with micro-electro-mechanical systems (MEMS), to probe living cells stiffness, have also been reported in the literature [196, 197]. They usually rely on the controlled displacement of a moving actuator compressing the cell against a fixed part. For example, Barazani et al. [197] developed a MEMS relying on an AC driven electrothermal micro-actuator to compress single yeast cells against a reference back spring. The motion of the reference spring divided by the cell deformation provides the cell stiffness relative to the reference spring constant. They report an average stiffness of the yeast cells of $9.3 \pm 3.1\ \mathrm{Nm}^{-1}$ and an average force necessary to rupture their membrane of $0.47 \pm 0.1\ \mu\mathrm{N}$. Gnerlich et al. [196] have worked on a similar MEMS and they have reported the compression of NIH 3T3 mouse fibroblasts by moving the actuator by 4 μm for 90 s using a calibrated piezo-driver. They have measured the associated forces decreased during the compression from 38 to 5 nN, which is well described by a viscoelastic cell model. Finally, we can cite the work from Lafitte et al. [198] presenting the utilization of silicon nano-tweezers (SNT) to probe the mechanical properties of biological samples (DNA and cells). Typically, one tip of the tweezer can be alternatively open and closed to compress the cell and the other one is fixed and senses the absolute force applied. The mechanical response of the cells can be deduced in real-time from the changes of the resonance frequency of the SNT, knowing that the resonance response changes according to the added rigidity and

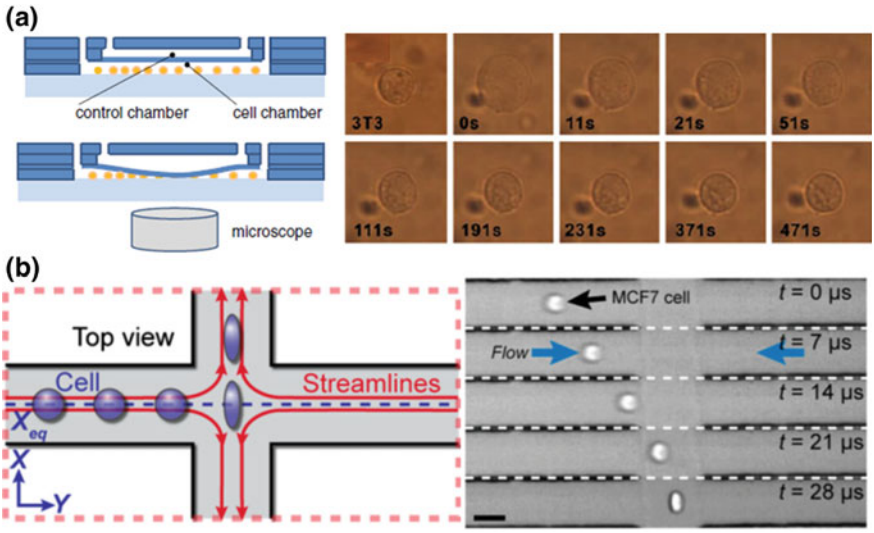

Fig. 4.22 **a** Schematic of the principle of compression experiements. Sequence of relaxation of a 3T3 cell after compression is stopped (Reproduced from [193], copyright The authors (2010), with permission of Springer). **b** Schematic view and sequence of deformation of a focused cell being stretched when entering the extensional flow region (Reproduced with permission from [195])

viscosity of the cell. However, the use of MEMS to characterize the mechanical phenotype of cells over a large cell population remains to be demonstrated.

4.4.3.4 Fluid-Based Deformability Assays

Perhaps the simplest method to measure cellular mechanical properties while achieving high-throughput is by monitoring cell deformations as they flow through microfluidic channels. Cellular deformability can be challenged either by the walls of the device or by the associated shear stress without any contact, thus limiting the impact of cell membrane adhesion with channel boundaries. Microfluidic deformability-based passive separation techniques can also be used to characterize mechanical phenotype of cells. Such techniques have been detailed in Sect. 4.3 and therefore will not be addressed again here.

Fluid stretching. RBCs are highly deformable and their deformability can therefore be challenged using shear stress generated by microfluidic channels wider than the typical size of the cell. Forsyth et al. [199] reported three different dynamic behaviors of RBCs in a pressure-driven flow, according to the shear rate: stretching, tumbling and recoiling. Upon chemical treatment with glutaraldehyde, which is known to rigidify both cell membrane and cytoplasm, RBCs presented lower deformation and increased occurrence of tumbling, which is a motion typical of rigid bodies. Lee et al. [200] reported the monitoring of RBC deformation in a

hyperbolic converging microchannel. They showed that the extensional flow is more efficient to induce cell deformation than a shear flow, as RBCs presented deformation index of 0.51 and 0.29 at 3 Pa respectively. Such approach was used to detect the decrease in deformability of RBCs following heat treatment.

Gosset et al. [195] proposed an automated microfluidic tool using inertial focusing to uniformly deliver cells to a stretching extensional flow where cells are deformed at high strain rates (Fig. 4.22b). They characterized the deformability of populations of leukocytes and malignant cells in pleural fluid samples. They predicted disease state in patients with cancer and immune activation with a sensitivity of 91% and a specificity of 86% at high throughput (2000 cells/s). Both lymphocyte activation and stem cell pluripotency were found to be associated with increased deformability [195].

Constriction channels. Constriction channels with dimensions smaller than the typical size of a single cell provide a simple and powerful tool to probe cell deformability. Several types of geometric restrictions have been reported in the literature to quantify cell mechanical phenotype, using however the same type of readout (transit time, deformation index and relaxation time). For example Selby et al. [201] reported the use of a well-defined geometrical constriction ranging from 8 to 2 μm in width and controlled pressure gradients in order to discriminate healthy and malaria-iRBCs. They report that as parasites develop within the host cell, the increase of RBCs rigidity prevent their passage through smaller constrictions. Indeed Fig. 4.23a illustrates the blockage of a 6 μm wide channel by schizontes-iRBCs, whereas a hRBC (in red) manages to deform past the barricade. Using the same approach, Suresh [180] probed the mechanical properties of human pancreatic cells flowing in a microfluidic channel at 0.5 μL/min (Fig. 4.23b). By studying transit velocity measurements, shape change and relaxation at the exit of the narrowing, they connected changes in cell deformability and motility [180]. The distinction between non-malignant and cancerous cells flowing in similar geometries was demonstrated using entry time [202, 203]—defined as the time necessary for the cell to deform and enter completely into the microchannel—and deformation index measurements [203].

Flow of cells in 16 parallel channels implementing multiple constrictions has also been reported (Fig. 4.23c) [204]. The study revealed that transit time scales indeed with cell size and that simultaneous transit events occurring across neighboring constrictions can influence transit time [204]. A comparable geometry was used to quantify the effect of taxol—an anti-cancer drug—on the transit time of tumor cells [207] through the serial constrictions. The results show that when travelling through the first constriction, cells treated with taxol undergo longer transit times than untreated cells, however for subsequent transits the difference was smaller between the two groups [207]. Rosenbluth et al. [208] measured single-cell transit times of white blood cell populations passing through in vitro capillary networks, allowing to observe several channels in parallel. They demonstrate clinical relevance of their geometry in sepsis and leukostasis, showing increased transit time with patient samples relative to control ones. Their results also revealed that chemotherapy reduce leukemia cell deformability [209]. Herricks et al. [210] reported that

ring-iRBCs get blocked upstream whereas hRBCs reached positions further downstream in converging channels. The dynamic behavior of RBCs flowing through arrays of 15 µm pillars, either slowly through 5–2 µm wide gaps or rapidly along 10 µm wide channels has been studied [211]. They observed that mechanically impaired RBCs—either due to heat treatment or issued from malaria-iRBCs or from patients with hereditary spherocytosis—tend to accumulate in narrow slits more frequently than normal RBCs, hence demonstrating their increased rigidity. The same approach was used by Preira et al. [205] to explore the effect of actin organization and miosin II on the deformability of leukocytes using pore-based deformability measurement (Fig. 4.23d). They highlighted that cell stiffness

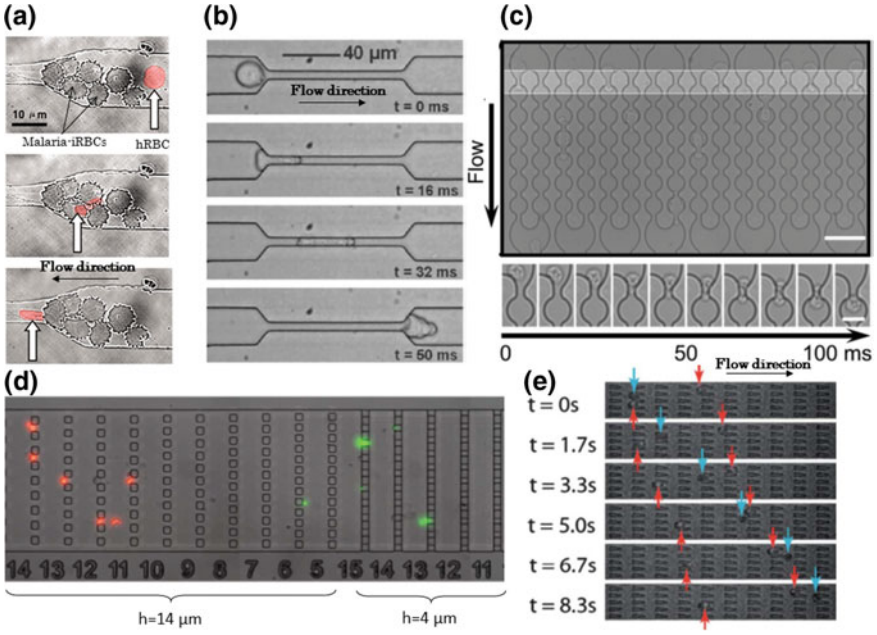

Fig. 4.23 **a** Video-microscopic images showing malaria-iRBCs being stuck at the entry of a geometric narrowing, whereas a helathy cell (in red) managed to deform past the blockage (Reproduced with permission from [201], copyright (2003) National Academy of Sciences, U.S. A.). **b** Sequence of deformation of a human pancreatic tumor cell flowing through a constriction (Reproduced from [180], copyright (2007) with permission of Elsevier). **c** Image of the multi-constriction array, which consist in 16 channels each implementing a series of 5 constrictions. Sequence of deformation of a single HL-60 cell during flow through a 5 µm constriction; transit time of 80 ms is measured (Reproduced from [204] with permission of the Royal Society of Chemistry). **d** Illustration of the deformability-based separation. Stiff THP-1 cells (treated by glutaraldehyde) labelled in red are trapped in larger pores than compliant THP-1 cells (treated by Latrunculin-A) labelled in green (Reproduced from [205] with permission of the Royal Society of Chemistry). **e** Time-lapse images of ring stage-iRBCs (red arrows) and hRBCs (blue arrows) flowing in the device; the hRBC travels faster than the iRBC (Reproduced from [206] with permission of the Royal Society of Chemistry)

depends mainly on actin organization, whereas shape is related to miosin II. Similarily, Bow et al. [206] have monitored dynamic mechanical responses of 10^3–10^4 individual RBCs using converging or diverging obstacles (Fig. 4.23e). They have experimentally demonstrated that differences in RBC deformability, demonstrated by differences in transit velocity, are enhanced in geometries with sharper corners, for a given pressure difference. The influence of an anti-malaria drug (Artesunate) on the dynamic deformability of ring-infected iRBCs was also evaluated [212]. After Artesunate treatment, they observed a 50% decrease in the transit velocity of iRBCs whereas only 10% in speed reduction is observed for hRBCs.

A limitation to constriction channels however is the influence of size and adhesiveness on cells behavior, which makes it difficult to emphasize the role of deformability alone. Indeed, recent studies trying to take the cell size into account have been reported in the literature [213]. They showed that cell size significantly influences travel times and that for a given volume, stiffer cells have longer transit times than compliant ones. However, efforts still need to be made to characterize adhesion and/or friction between channel walls and cell membrane, for example by varying the walls coating. Nyberg et al. [204] have reported variability in transit time measurements as the PDMS device age after plasma treatment; they attribute such discrepancies to modifications in channel surface properties. Another drawback of this approach is the need to adapt precisely the size of the constriction to dimensions of cells of interest to avoid clogging or deform significantly the cells.

Pressure drop measurements. Abkarian et al. [214, 215] proposed a high-speed microfluidic approach to measure dynamical pressure-drop variations associated with the flow of individual cells in confined geometries. The chip is composed of two identical channels (picture in Fig. 4.24a); the cells suspension is injected in the upper channel whereas a solution of contrast agent is injected in the lower one. The two channels merge on the right side of the chip and the contrast agent allow the visualization of the co-flow virtual interface. In absence of cells flowing in the upper channel, the virtual interface is centered, hence traducing the equilibrium between the pressures in the two channels. When a deformable cell enters the upper channel, an additional hydrodynamic resistance is added to the channel resistance, leading to changes in the local pressure profile, thus inducing a displacement of the virtual interface. Thanks to an appropriate calibration, the deflation of the interface can be converted into a pressure drop measurement. The authors have shown that the amplitude of pressure drop depends on both the volume and the deformability (graph in Fig. 4.24a) of the cells under study. Indeed, pressure-drop measurements are able to discriminate WBCs and RBCS, as well as healthy and chemically rigidified RBCs [214]. Khan et al. [203] applied this approach to the mechanical characterization of healthy and cancerous brain cells. The two cell lines were differentiated using entry time and to a little extend pressure drops, rather than on speeds and elongations. They observed that brain tumor cells have a longer entry time, thus suggesting that the well-spread idea that cancer cells are more deformable than benign cells may not apply to brain cancer cells [203].

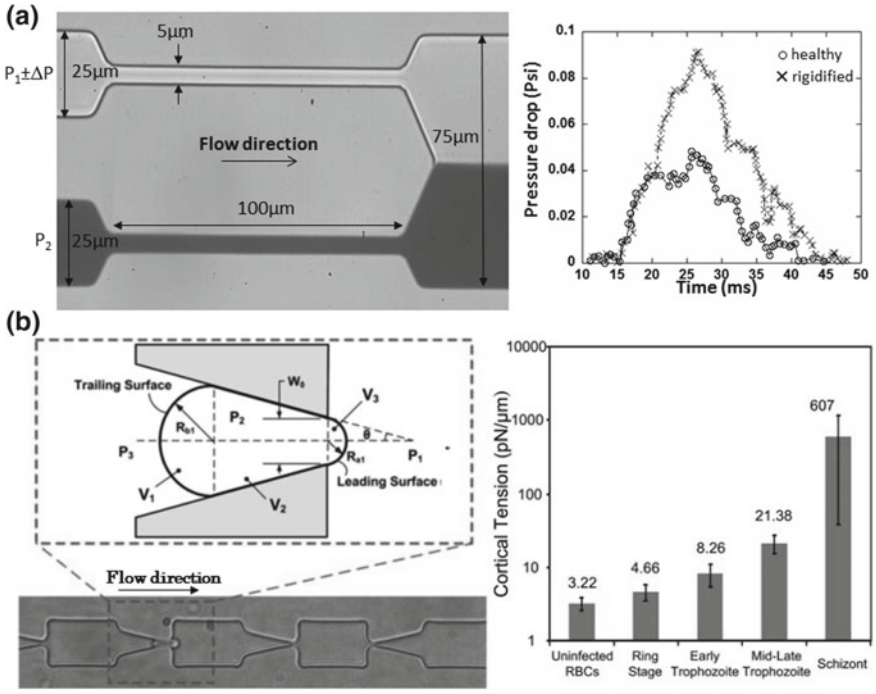

Fig. 4.24 **a** Pressure drop measurements rely on the geometry of the device. The monitoring of the displacement of the virtual interface in the co-flow region of the chip is correlated to the pressure drop associated with the flow of a cell in the upper channel. Pressure drop versus time for (×) a hRBC and (o) a rigidified RBC after 0.001% glutaraldehyde treatment. **b** Microfluidic adaptation of the micropipette aspiration technique. RBCs are deformed when passing the funnel constriction and the associated geometric model. Measured cortical tension of hRBCs and malaria-iRBCs in various stages of infection (reproduced from [216] with permission of the Royal Society of Chemistry)

Microfluidic micropipette aspiration. Guo et al. [216] proposed an adaptation of the conventional micropipette aspiration technique into microfluidic format. Figure 4.24b presents the geometry of the microfluidic micropipette aspiration device implementing multiple funnel-shaped constrictions with openings ranging from 5 down to 1 µm. As a cell is flowing in the device, it gets trapped at the nozzle of a funnel, the pressure difference is manually increased until the RBC is allowed to squeeze past the restriction. The threshold pressure is used to determine the intrinsic stiffness of each cell. Using the same mathematical model as in conventional pipette aspiration technique, i.e. considering the RBC as a liquid-drop with constant volume, they managed to extract the cell cortical tension. Malaria-iRBCs by early (ring) through late (schizont) developmental stages of the parasite were shown to be 1.5 to 200-fold stiffer than uninfected cells (graph in Fig. 4.24b) as already reported in the literature [217]. However, the rectangular cross-section of

the geometry can rise concerns about the validity of applying conventional micropipette models to retrieve cellular mechanical properties.

4.4.4 Conclusion

Although they present many advantages such as possible automation, absence of labeling and compatibility with high throughput, each microfluidic mechanical characterization technique has some drawbacks. In optical stretching, cells are exposed to the power of the laser which may damage them and electro-deformation require a change in suspending media; such low conductivity buffer may accelerate aging of the cells. Multi-steps soft lithography processes are needed to implement the flexible membrane in compression experiments. A disadvantage of constriction channels is the persistent possibility of device clogging. Indeed, as the section of the constriction is smaller than the typical size of the cells, one need to adapt carefully the width of the constriction. A group proposed recently an improvement with the development of a constriction channel with tunable section [218, 219]. One of the walls of the constriction was replaced by a thin membrane, which deflection is controlled via external pressure. In case of channel obstruction by larger particles or cellular aggregates, the increase of the applied pressure causes the augmentation of the constriction cross-section through deflection of the membrane, thus removing the obstruction.

Up to recently, the various techniques presented above presented the same limitation in terms of throughput because of the use of high-speed video-microscopy for monitoring cellular mechanical responses such as the deformation index. Indeed, even when using automated post-processing routines, the huge amount of image data to analyze imposes computational power and remains time consuming. In replacement of high-speed camera, electrical impedance measurements has been reported in the literature to detect RBCs [220] and cancer cells [213] deformation in constriction channels, with a throughput of 100 cells/s. In 2015, Jochen Guck's group has proposed an automated real-time deformability cytometer (RTDT) able to perform continuous cell mechanical characterization of large populations (above 100 000 cells) with throughput greater than 100 cells/s [221, 222]. Their system consists in the real-time measurement of the deformation associated with the passage of cells into a constriction channel. They report that RT-DC is sensitive to cytoskeletal alterations and can distinguish cell-cycle phases, track stem cell differentiation into distinct lineages and identify cell populations in whole blood by their mechanical fingerprints. More recently, Deng and Chung [223] proposed a similar device allowing nearly real-time analysis of transient deformation of cells hitting a wall at a T-junction. Their automated process allow the mechanical characterization of cells at a throughput of 2000 cells/s. Finally, the last challenge that still need to be addressed is the translation of raw parameters such as entry time or deformation index into cellular intrinsic mechanical characteristics such as Young's modulus or cortical tension. Indeed, intrinsic deformability parameters are independent of the setup

(viscosity, flow speed, etc.…) and allow the comparison of data obtained with various techniques and by various research groups. Therefore there is a strong need for theoretical framework and mechanical modeling of the cellular response in order to extract intrinsic mechanical properties.

References

1. T. Vilkner, D. Janasek, A. Manz, Micro total analysis systems. Recent developments. Anal. Chem. **76**, 3373–3386 (2004). Accessed 01 June 2004
2. H.A. Stone, A.D. Stroock, A. Ajdari, Engineering flows in small devices. Ann. Rev. Fluid Mech. **36**, 381–411 (2004)
3. A. Boisen, S. Dohn, S.S. Keller, S. Schmid, M. Tenje, Cantilever-like micromechanical sensors. Rep. Progr. Phys. **74**, 036101 (2011). Accessed 01 Mach 2011
4. G.T. Kovacs, *Micromachined Transducers Sourcebook*, 1st edn. (McGraw-Hill Science/Engineering/Math, Boston, 1998)
5. K.W. Oh, C. Park, K. Namkoong, A world-to-chip microfluidic interconnection technology with dual functions of sample injection and sealing for a multichamber micro PCR chip, in *18th IEEE International Conference on Micro Electro Mechanical Systems, MEMS 2005* (2005), pp. 714–717
6. K.I.T.H.K. Nkashima, 10-way micro switching valve chip for multi-directional flow control (2003)
7. M.T. Taylor, P. Nguyen, J. Ching, K.E. Petersen, Simulation of microfluidic pumping in a genomic DNA blood-processing cassette. J. Micromech. Microeng. **13**, 201 (2003)
8. M.A. Unger, H.-P. Chou, T. Thorsen, A. Scherer, S.R. Quake, Monolithic microfabricated valves and pumps by multilayer soft lithography. Science, **288**, 113–116 (2000). Accessed 07 April 2000
9. V. Studer, G. Hang, A. Pandolfi, M. Ortiz, W.F. Anderson, S.R. Quake, Scaling properties of a low-actuation pressure microfluidic valve. J. Appl. Phys. **95**, 393–398 (2004) 01 Jan 2004
10. A. Pandolfi, M. Ortiz, Improved design of low-pressure fluidic microvalves. J. Micromech. Microeng. **17**, 1487 (2007)
11. K.W. Oh, C.H. Ahn, A review of microvalves. J. Micromech. Microeng. **16**, R13 (2006)
12. Mechanics over micro and nano scales (Springer, New York, 2011)
13. B. Bae, N. Kim, H. Kee, S.-H. Kim, Y. Lee, S. Lee et al. Feasibility test of an electromagnetically driven valve actuator for glaucoma treatment. J. Microelectromech. Syst. **11**, 344–354 (2002)
14. K.W. Oh, A. Han, S. Bhansali, C.H. Ahn, A low-temperature bonding technique using spin-on fluorocarbon polymers to assemble microsystems. J. Micromech. Microeng. **12**, 187 (2002)
15. S.C. Terry, J.H. Jerman, J.B. Angell, A gas chromatographic air analyzer fabricated on a silicon wafer. IEEE Trans. Electron Devices **26**, 1880–1886 (1979)
16. K. Sato, M. Shikida, An electrostatically actuated gas valve with an S-shaped film element. J. Micromech. Microeng. **4**, 205 (1994)
17. M. Patrascu, J. Gonzalo-Ruiz, M. Goedbloed, S.H. Brongersma, M. Crego-Calama, Flexible, electrostatic microfluidic actuators based on thin film fabrication. Sens. Actuat. A Phys. **186** 249–256 (2012)
18. W. van der Wijngaart, H. Ask, P. Enoksson, G. Stemme, A high-stroke, high-pressure electrostatic actuator for valve applications. Sens. Actuat. A Phys. 100, 264–271 (2002). Accessed 01 Sep 2002

19. S. Messner, J. Schaible, H. Sandmaier, and R. Zengerle, Three-way silicon microvalve for pneumatic applications with electrostatic actuation principle, Microfluid. Nanofluid. **2**, 89–96 (2005). Accessed 28 July 2005
20. T. Ninomiya, Y. Okayama, Y. Matsumoto, X. Arouette, K. Osawa, N. Miki, MEMS-based hydraulic displacement amplification mechanism with completely encapsulated liquid. Sens. Actuat. A: Phys. **166**, 277–282 (2011)
21. E.-H. Yang, C. Lee, J. Mueller, T. George, Leak-tight piezoelectric microvalve for high-pressure gas micropropulsion. J. Microelectromech. Syst. **13**, 799–807 (2004)
22. T. Goettsche, J. Kohnle, M. Willmann, H. Ernst, S. Spieth, R. Tischler et al. Novel approaches to particle tolerant valves for use in drug delivery systems. Sens. Actuat. A Phys. **118**, 70–77 (2005). Accessed 31 Feb 2005
23. P. Ivaldi, J. Abergel, M.H. Matheny, L.G. Villanueva, R.B. Karabalin, M.L. Roukes et al., 50 nm thick AlN film-based piezoelectric cantilevers for gravimetric detection. J. Micromech. Microeng. **21** (2011)
24. T. Rogge, Z. Rummler, W.K. Schomburg, Polymer micro valve with a hydraulic piezo-drive fabricated by the AMANDA process. Sens. Actuat. A Phys. **110**, 206–212 (2004). Accessed 01 Feb 2004
25. H. Jerman, Electrically activated normally closed diaphragm valves. J. Micromech. Microeng. **4**, 210 (1994)
26. D.J. Leo, Engineering analysis of smart material systems, in *Engineering Analysis of Smart Material Systems* (Wiley, 2007), pp. i–xiv
27. M. Kohl, D. Dittmann, E. Quandt, B. Winzek, Thin film shape memory microvalves with adjustable operation temperature. Sens. Actuat. A Phys. **83**, 214–219 (2000). Accessed 22 May 2000
28. H. Takao, K. Miyamura, H. Ebi, M. Ashiki, K. Sawada, and M. Ishida, A MEMS microvalve with PDMS diaphragm and two-chamber configuration of thermo-pneumatic actuator for integrated blood test system on silicon. Sens. Actuat. A Phys. **119**, 468–475 (2005). Accessed 13 April 2005
29. C. Goll, W. Bacher, B. Büstgens, D. Maas, W. Menz, W.K. Schomburg, Microvalves with bistable buckled polymer diaphragms. J. Micromech. Microeng. **6**, 77 (1996)
30. A. Chen, T. Pan, Manually operatable on-chip bistable pneumatic microstructures for microfluidic manipulations. Lab Chip **14**, 3401–3408 (2014). Accessed 31 July 2014
31. C. Megnin, J. Barth, M. Kohl, A bistable SMA microvalve for 3/2-way control. Sens. Actuat. A Phys. **188**, 285–291 (2012)
32. B. Yang, B. Wang, W.K. Schomburg, A thermopneumatically actuated bistable microvalve. J. Micromech. Microeng. **20**, 095024 (2010)
33. A.K. Au, H. Lai, B.R. Utela, A. Folch, Microvalves and micropumps for BioMEMS. Micromachines **2**, 179–220 (2011). Accessed 24 May 2011
34. J. Voldman, M.L. Gray, M.A. Schmidt, An integrated liquid mixer/valve. J. Microelectromech. Syst. **9**, 295–302 (2000)
35. J. Kim, J. Baek, K. Lee, Y. Park, K. Sun, T. Lee et al., Photopolymerized check valve and its integration into a pneumatic pumping system for biocompatible sample delivery. Lab Chip **6**, 1091–1094 (2006). Accessed 26 July 2006
36. G.-H. Feng, E.S. Kim, Micropump based on PZT unimorph and one-way parylene valves. J. Micromech. Microeng. **14**, 429 (2004)
37. C.A. Hufnagel, W.P. Harvey, P.J. Rabil, T.F. McDermott et al. Surgical correction of aortic insufficiency. Surgery **35**, 673–683 (1954)
38. A. Starr, M.L. Edwards, Mitral replacement: clinical experience with a ball-valve prosthesis. Ann. Surg. **154**, 726–740 (1961)
39. Prosthetic Heart Valves: Practice Essentials, Background, Design Features 35 (2017). Accessed 09 March 2017
40. E.F. Hasselbrink, T.J. Shepodd, J.E. Rehm, High-pressure microfluidic control in lab-on-a-chip devices using mobile polymer monoliths. Anal. Chem. **74**, 4913–4918 (2002). 01 Oct 2002

41. V. Seidemann, S. Bütefisch, S. Büttgenbach, Fabrication and investigation of in-plane compliant SU8 structures for MEMS and their application to micro valves and micro grippers. Sens. Actuat. A Phys. **97–98**, 457–461 (2002), 2002/04/01
42. A. Nisar, N. Afzulpurkar, B. Mahaisavariya, A. Tuantranont, MEMS-based micropumps in drug delivery and biomedical applications, Sens. Actuat. B Chem. 130, pp. 917–942, 2008/ 03/28/ 2008
43. G. Destgeer, H.J. Sung, Recent advances in microfluidic actuation and micro-object manipulation via surface acoustic waves. Lab Chip (2015). Accessed 28 May 2015
44. D.J. Laser, J.G. Santiago, A review of micropumps, J. Micromech. Microeng. **14**, R35 (2004)
45. R. Hebden, A.M. Baker, L. Stenmark, J. Köhler, J.L. Moerel, W. Halswijk, Towards the development of a monopropellant microrocket engine using MEMS technology. ResearchGate
46. J.K. Igor, P.M. Joseph, C. Paul, C.H. Charles, Classification of pumps, in *Pump Handbook,* Fourth edn (McGraw Hill Professional, Access Engineering, 2008)
47. M. Richter, R. Linnemann, P. Woias, Eurosensors XIRobust design of gas and liquid micropumps. Sens. Actuat. A: Phys. **68**, 480–486 (1998). Accessed 15 June 1998
48. H.T.G. Van Lintel, F.C.M. Van de Pol, S. Bouwstra, A piezoelectric micropump based on micromachining of silicon. Sens. Actuat. **15**, 153–167 (1988)
49. J.G. Smits, Proceedings of the 5th International Conference on Solid-State Sensors and Actuators and Eurosensors IIIPiezoelectric micropump with three valves working peristaltically. Sens. Actuat. A Phys. **21**, 203–206 (1990). Accessed 01 Feb 1990
50. S. Shoji, S. Nakagawa, M. Esashi, Proceedings of the 5th International Conference on Solid-State Sensors and Actuators and Eurosensors IIIMicropump and sample-injector for integrated chemical analyzing systems. Sens. Actuat. A Phys. **21**, 189–192 (1990). Accessed 01 Feb 1990
51. C. Yamahata, F. Lacharme, Y. Burri, M.A.M. Gijs, A ball valve micropump in glass fabricated by powder blasting. Sens. Actuat. B Chem. **110**, 1–7 (2005). Accessed 30 Sep 2005
52. B. Cetin, R. Salemmilani, D. Li, Microfluidic Rotary Pump, in *Encyclopedia of Microfluidics and Nanofluidics*, ed. by D. Li (Springer, New York, 2013), pp. 1–6
53. M. Ashouri, M.B. Shafii, A. Moosavi, H. Amiri Hezave (2015) A novel revolving piston minipump. Sens. Actuat. B Chem. **218**, 237–244. Accessed 31 Oct 2015
54. H.-P. Chou, M.A. Unger, S.R. Quake, A microfabricated rotary pump. Biomed. Microdevices **3**, 323–330 (2001)
55. A.R. Tovar, A.P. Lee, Lateral cavity acoustic transducer. Lab Chip **9**, 41–43 (2009). Accessed 07 Jan 2009
56. M.V. Patel, A.R. Tovar, A.P. Lee, Lateral cavity acoustic transducer as an on-chip cell/ particle microfluidic switch. Lab Chip **12**, 139–145 (2012)
57. J.P. Brody, P. Yager, R.E. Goldstein, R.H. Austin, Biotechnology at low Reynolds numbers. Biophys. J. **71**, 3430–3441 (1996). Accessed 12 1996
58. Z. Guttenberg, H. Müller, H. Habermüller, A. Geisbauer, J. Pipper, J. Felbel et al., Planar chip device for PCR and hybridization with surface acoustic wave pump. Lab Chip **5**, 308–317 (2005). Accessed 22 Feb 2005
59. M. Plodinec, M. Loparic, C.A. Monnier, E.C. Obermann, R. Zanetti-Dallenbach, P. Oertle et al. The nanomechanical signature of breast cancer. Biophys. J. **104**, 321a (2013). Accessed 29 Jan 2013
60. Y. Nematbakhsh, C.T. Lim, Cell biomechanics and its applications in human disease diagnosis. Acta Mech. Sin. **31**, 268–273 (2015). Accessed 12 May 2015
61. J. Tamayo, P.M. Kosaka, J.J. Ruz, A. San Paulo, M. Calleja, Biosensors based on nanomechanical systems. Chem. Soc. Rev. **42**, 1287–1311 (2013)
62. M. Calleja, P.M. Kosaka, Á.S. Paulo, J. Tamayo, Challenges for nanomechanical sensors in biological detection. Nanoscale **4**, 4925–4938 (2012). Accessed 27 June 2012

63. A. Gupta, D. Akin, R. Bashir, Single virus particle mass detection using microresonators with nanoscale thickness. Appl. Phys. Lett. **84**, 1976–1978 (2004). Accessed 15 March 2004
64. G. Villanueva, F. Perez-Murano, M. Zimmermann, J. Lichtenberg, J. Bausells, "Piezoresistive cantilevers in a commercial CMOS technology for intermolecular force detection. Microelectron. Eng. **83**, 1302–1305, April–Sep 2006
65. G. Villanueva, J.A. Plaza, J. Montserrat, F. Perez-Murano, J. Bausells, Crystalline silicon cantilevers for piezoresistive detection of biomolecular forces. Microelectron. Eng. **85**, 1120–1123 (2008)
66. J. Tamayo, P. M. Kosaka, J.J. Ruz, Á.S. Paulo, M. Calleja, Biosensors based on nanomechanical systems. Chem. Soc. Rev. **42**, 1287–1311 (2013). Accessed 16 Jan 2013
67. J.L. Arlett, E.B. Myers, M.L. Roukes,Comparative advantages of mechanical biosensors. Nat. Nanotechnol. **6**, 203–215, (2011). Accessed April 2011
68. G. Tosolini, G. Villanueva, F. Perez-Murano, J. Bausells, Silicon microcantilevers with MOSFET detection. Microelectron. Eng. **87**, 1245–1247, May–Aug 2010
69. G. Villanueva, J. Montserrat, F. Perez-Murano, G. Rius, J. Bausells, Submicron piezoresistive cantilevers in a CMOS-compatible technology for intermolecular force detection. Microelectron. Eng. **73–4**, 480–486 (2004)
70. J. Tamayo, J. J. Ruz, V. Pini, P. Kosaka, and M. Calleja, Quantification of the surface stress in microcantilever biosensors: revisiting Stoney's equation. Nanotechnology **23**,475702 (2012)
71. V. Pini, J.J. Ruz, P.M. Kosaka, O. Malvar, M. Calleja, J. Tamayo, How two-dimensional bending can extraordinarily stiffen thin sheets. Sci. Rep. **6**. Accessed 11 July 2016
72. J. Fritz, M.K. Baller, H.P. Lang, H. Rothuizen, P. Vettiger, E. Meyer et al., Translating biomolecular recognition into nanomechanics. Science **288**, 316–318 (2000)
73. D. Ramos, J. Tamayo, J. Mertens, M. Calleja, L.G. Villanueva, A. Zaballos, Detection of bacteria based on the thermomechanical noise of a nanomechanical resonator: origin of the response and detection limits. Nanotechnology **19**, 035503 (2008). Accessed 23 Jan 2008
74. E.A. Corbin, F. Kong, C.T. Lim, W.P. King, R. Bashir, Biophysical properties of human breast cancer cells measured using silicon MEMS resonators and atomic force microscopy. Lab Chip **15**, 839–847 (2015). Accessed 22 Jan 2015
75. K.L. Ekinci, M.L. Roukes, Nanoelectromechanical systems. Rev. Sci. Instrum. **76**, 061101 (2005). Accessed 01 June 2005
76. M. Sansa, E. Sage, E.C. Bullard, M. Gely, T. Alava, E. Colinet et al., Frequency fluctuations in silicon nanoresonators. Nat. Nanotechnol. **11**, 552 (2016)
77. K.Y. Gfeller, N. Nugaeva, M. Hegner, Rapid biosensor for detection of antibiotic-selective growth of escherichia coli. Appl. Environ. Microbiol. **71**, 2626–2631 (2005). Accessed 01 May 2005
78. M.K. Ghatkesar, T. Braun, V. Barwich, J.-P. Ramseyer, C. Gerber, M. Hegner et al., Resonating modes of vibrating microcantilevers in liquid. Appl. Phys. Lett. **92**, 043106 (2008). Accessed 28 Jan 2008
79. E. Oesterschulze, P. Kehrbusch, B. Radzio, E. A. Ilin, A. Thyssen, J. W. Deitmer et al., Tailoring the interface of hybrid microresonators in viscid fluids enhances their quality factor by two orders of magnitude. Lab on a Chip **12**, 1316–1319 (2012). Accessed 07 March 2012
80. M. Melli, G. Scoles, M. Lazzarino, Fast detection of biomolecules in diffusion-limited regime using micromechanical pillars. ACS Nano **5**, 7928–7935 (2011). Accessed 25 Oct 2011
81. D. Ziegler, P.D. Ashby, Encased cantilevers for ultra-low-noise force spectroscopy of proteins and ligand receptor complexes. Biophys. J. **102**, 579a (2012). Accessed 31 Jan 2012
82. T.P. Burg, S.R. Manalis, Suspended microchannel resonators for biomolecular detection. Appl. Phys. Lett. **83**, 2698–2700 (2003). Accessed 29 Sep 2003
83. M. Rodahl, F. Höök, A. Krozer, P. Brzezinski, B. Kasemo, Quartz crystal microbalance setup for frequency and Q-factor measurements in gaseous and liquid environments. Rev. Sci. Instrum. **66**, 3924–3930 (1995). Accessed 01 July 1995

84. S.K. Vashist, P. Vashist, Recent advances in quartz crystal microbalance-based sensors. J. Sens. e571405 (2011), 19 Sep 2011
85. N. Kim, D.-K. Kim, Y.-J. Cho, Development of indirect-competitive quartz crystal microbalance immunosensor for C-reactive protein. Sens. Actuat. B Chem. **143**, 444–448 (2009). Accessed 04 Dec 2009
86. K. Länge, B.E. Rapp, M. Rapp, Surface acoustic wave biosensors: a review. Anal. Bioanal. Chem. **391**, 1509–1519 (2008). Accessed 12 Feb 2008
87. N.G. Durmuş, R.L. Lin, M. Kozberg, D. Dermici, A. Khademhosseini, U. Demirci, Acoustic-based biosensors, in *Encyclopedia of Microfluidics and Nanofluidics* ed. by D. Li (Springer, New York, 2015), pp. 28–40
88. S.U. Senveli, Z. Ao, S. Rawal, R.H. Datar, R.J. Cote, O. Tigli, A surface acoustic wave biosensor for interrogation of single tumour cells in microcavities **16**, 163–171 (2015). Accessed 15 Dec 2015
89. Oscillating U-tube, in *Wikipedia* (2016)
90. S. Byun, S. Son, D. Amodei, N. Cermak, J. Shaw, J. H. Kang et al., Characterizing deformability and surface friction of cancer cells. Proc. Natl. Acad. Sci. **110**, 7580–7585 (2013). Accessed 07 May 2013
91. N. Cermak, S. Olcum, F.F. Delgado, S.C. Wasserman, K.R. Payer, M.A. Murakami et al., High-throughput measurement of single-cell growth rates using serial microfluidic mass sensor arrays. Nat. Biotechnol. (2016). Advance online publication. Accessed 05 Sep 2016
92. A.K. Bryan, V.C. Hecht, W. Shen, K. Payer, W.H. Grover, S.R. Manalis, Measuring single cell mass, volume, and density with dual suspended microchannel resonators. Lab on a Chip **14**, 569–576 (2013). Accessed 23 Dec 2013
93. S. Olcum, N. Cermak, S.C. Wasserman, K.S. Christine, H. Atsumi, K.R. Payer et al., Weighing nanoparticles in solution at the attogram scale. Proc. Natl. Acad. Sci. **111**, 1310–1315 (2014). Accessed 28 Jan 2014
94. M.F. Khan, S. Schmid, P.E. Larsen, Z.J. Davis, W. Yan, E.H. Stenby et al., Online measurement of mass density and viscosity of pL fluid samples with suspended microchannel resonator. Sens. Actuat. B Chem. **185**, 456–461 (2013). Accessed Aug 2013
95. T.P. Burg, M. Godin, S.M. Knudsen, W. Shen, G. Carlson, J.S. Foster et al., Weighing of biomolecules, single cells and single nanoparticles in fluid. Nature **446**, 1066–1069 (2007). Accessed 26 April 2007
96. J.L. Arlett, M.L. Roukes, Ultimate and practical limits of fluid-based mass detection with suspended microchannel resonators. J. Appl. Phys. **108**, 084701 (2010). Accessed 15 Oct 2010
97. J. El-Ali, P.K. Sorger, K.F. Jensen, Cells on chips. Nature **442**, 403–411 (2006)
98. M. Cristofanilli, G.T. Budd, M.J. Ellis et al., Circulating tumor cells, disease progression, and survival in metastatic breast cancer. N. Engl. J. Med. **351**, 781791 (2004)
99. W.R. Rodriguez, N. Christodoulides, P.N. Floriano, S. Graham, M. Mohanty, M. Dixon, M. Hsiang, T. Peter, S. Zavahir, I. Thior, D. Romanovicz, B. Bernard, A.P. Goodey, B.D. Walker, J.T. McDevitt, A microchip CD4 counting method for HIV monitoring in resource-poor settings. PLoS Med **2**(7), 663–672 (2005)
100. X. Cheng, D. Irimia, M. Dixon et al., A microfluidic device for practical label-free CD4+ T cell counting of HIV-infected subjects. Lab Chip **7**(2), 170–178 (2007)
101. R. Huang, T.A. Barber, M.A. Schmidt, R.G. Tompkins, M. Toner, D.W. Bianchi, R. Kapur, W.L. Flejter, A microfluidics approach for the isolation of nucleated red blood cells (NRBCs) from the peripheral blood of pregnant women. Prenat. Diagn. **28**, 892899 (2008)
102. J. den Toonder, Circulating tumor cells: the grand challenge. Lab Chip **11**(3), 375–377 (2011)
103. R. David, M. Groebner, W.M. Franz, Magnetic cell sorting purification of differentiated embryonic stem cells stably expressing truncated human CD4 as surface marker. Stem Cells **23**(4), 477–482 (2005)

104. P. Gascoyne, C. Mahidol, M. Ruchirawat, J. Satayavivad, P. Watcharasit, F. Becker, Microsample preparation by dielectrophoresis: isolation of malaria. Lab Chip **2**(2), 70–75 (2002)
105. X. Xuan, J. Zhu, C. Church, Particle focusing in fluidic devices. Microfluid. Nanofluid. (2010). https://doi.org/10.1007/s10404-010-0602-7
106. A.A.S. Bhagat, H. Bow, H. Wei Hou, S. Jin Tan, J. Han, C. Teck Lim, Microfluidic for cell separation. Med. Biol. Eng. Comput. (2010). https://doi.org/10.1007/s11517-010-0611-4
107. C.W. Shields IV, C.D. Reyes, G.P. Lpez, Microfluidic cell sorting: a review of the advances in the separation of cells from debulking to rare cell isolation. Lab Chip (2015). https://doi.org/10.1039/c4lc01246a
108. J. Autebert, B. Coudert, F.C. Bidard, J.Y. Pierga, S. Descroix, L. Malaquin, J.L. Viovy, Microfluidic: an innovative tool for efficient cell sorting. Methods (2012). https://doi.org/10.1016/j.ymeth.2012.07.002
109. D.R. Gosset, W.M. Weaver, A.J. Mach, S.C. Hur, H.T. Kwong Tse, W. Lee, H. Amini, D. Di Carlo, Label-free cell separation and sorting in fluidic systems. Anal. Bioanal. Chem. (2010). https://doi.org/10.1007/s00216-010-3721-9
110. H. Ji, V. Samper, Y. Chen, C. Heng, T. Lim, L. Yobas, Silicon-based microfilters for whole blood cell separation. Biomed. Microdevices **10**, 251–257 (2008)
111. J. Han, B. Hansen, P. Abgrall, Continuous-flow deformability-based cell separation. Patent No. US20110081674 A1 (2011)
112. S.J. Tan, R.L. Lakshmi, P. Chen, W.T. Lim, L. Yabos, C.T. Lim, Versatile label free biochip for the detection of circulating tumor cells from peripheral blood in cancer patients. Biosens. Bioelectron. (2010). https://doi.org/10.1016/j.bios.2010.07.054
113. A. Yamada, S. Lee, P. Bassereau, C.N. Baroud, Trapping and release of Giant Unilamellar Vesicles in microfluidic wells. Soft Matter **10**, 5878–5885 (2014)
114. X. Fan, C. Jia, G. Li, H. Mao, Q. Jin, J. Zhao, A microfluidic chip integrated with a high-density PDMS-based microfiltration membrane for rapid isolation and detection of circulating tumor cells. Biosens. Bioelectron. **71**, 380–386 (2015)
115. J.P. Brody, T.D. Osborn, F.K. Forster, P. Yager, A planar microfabricated fluid filter. Sens. Actuat. A Phys. **54**, 704–708 (1996)
116. T.A. Crowley, V. Pizziconi, Isolation of plasma from whole blood using planar microfilters for lab-on-a-chip applications. Lab Chip (2005). https://doi.org/10.1039/b502930a
117. H. Mohamed, J.N. Turner, M. Caggana, Biochip for separating fetal cells from maternal circulation. J. Chromatogr. A **1162**(2), 187–192 (2007)
118. P. Sethu, A. Sin, M. Toner, Microfluidic diffusive filter for apheresis (leukapheresis). Lab Chip **6**, 83–89 (2006)
119. P. Wilding, L.J. Kricka, J. Cheng, G. Hvichia, M.A. Shoffner, P. Fortina, Integrated cell isolation and polymerase chain reaction analysis using silicon microfilter chambers. Anal. Biochem. (1998). https://doi.org/10.1006/abio.1997.2530
120. Y. Yoon, S. Kim, J. Lee, J. Choi, R.W. Kim, S.J. Lee, O. Sul, S.B. Lee, Clogging-free microfluidics for continuous size-based separation of microparticles. Scientific reports (2016). https://doi.org/10.1038/srep26531
121. D. Di Carlo, L.Y. Wu, L.P. Lee, Dynamic single cell culture array. Lab Chip **6**, 1445–1449 (2006)
122. J.A. Davis, D.W. Inglis, K.J. Morton, D.A. Lawrence, L.R. Huang, S.Y. Chou, J.C. Sturm, R.H. Austin, Deterministic hydrodynamics: taking blood apart. Proc. Natl. Acad. Sci. U.S.A **103**(40), 14779–14784 (2006)
123. S. Choi, S. Song, C. Choi, J.K. Park, Sheathless focusing of microbeads and blood cells based on hydrophoresis. Small **4**, 634–641 (2008)
124. D. Huh, J.H. Bahng, Y. Ling, H. Wei, O.D. Kripfgans, J.B. Fowlkes, J.B. Grotberg, S. Takayama, Gravity-driven microfluidic particle sorting device with hydrodynamic separation amplification. Anal. Chem. **79**, 1369–1376 (2007)

125. M. Yamada, K. Kano, Y. Tsuda, J. Kobayashi, M. Yamato, M. Seki, T. Okano, Microfluidic devices for size-dependent separation of liver cells. Biomed. Microdevices **9**(5), 637–645 (2007)
126. J. Takagi, M. Yamada, M. Yasuda, M. Seki, Continuous particle separation in a microchannel having asymmetrically arranged multiple branches. Lab Chip **5**, 778 (2005)
127. Z. Wu, B. Willing, J. Bjerketorp, J.K. Jansson, K. Hjort, Soft inertial microfluidics for high throughput separation of bacteria from human blood cells. Lab Chip **9**(9), 1193–1199 (2009)
128. D. Di Carlo, D. Irimia, R.G. Tompkins, M. Toner, Continuous inertial focusing, ordering and separation of particles in microchannels. Proc. Natl. Acad. Sci. U.S.A **104**(48), 18892–18897 (2007)
129. M. Faivre, M. Abkarian, K. Bickraj, H.A. Stone, Geometrical focusing of cells in a microfluidic device: an approach to separate blood plasma. Biorheology **43**(2), 147–159 (2006)
130. A. Jain, L.L. Munn, Biomimetic postcapillary expansions for enhancing rare blood cell separation on a microfluidic chip. Lab Chip **11**, 2941–2948 (2011)
131. S. Yang, A. Undar, J.D. Zahn, A microfluidic device for continuous, real time blood plasma separation. Lab Chip **6**(7), 871–880 (2006)
132. J.P. Beech, Microfluidics separation and analysis of biological particles. Ph.D. Thesis, Lund University, Sweeden (2011), https://tegen.ftf.lth.se/files/theses/beech2011.pdf
133. P. Beech, S.H. Holm, K. Adolfsson, J.O. Tegenfeldt, Sorting cells by size, shape and deformability. Lab Chip **12**, 1048–1051 (2012)
134. N. Tottori, Y. Sakurai, T. Nisisako, Y. Tanagida, T. Hatsuzawa, Thermally tunable deterministic lateral displacement through hydrogel micro pillar arrays. in *Proceedings of 20th International Conference on Miniaturized Systems for Chemistry and Life Sciences*, 9–13 October 2016, Dublin, Ireland (2016), pp. 140–141
135. D.W. Inglis, J.A. Davis, R.H. Austin, J.C. Sturm, Critical particle size for fractionation by deterministic lateral displacement. Lab Chip **6**, 655–658 (2006)
136. S.H. Holm, J.P. Beech, M.P. Barrett, J.O. Tegenfeldt, Separation of parasites from human blood using deterministic lateral displacement. Lab Chip **11**(7), 1326–1332 (2011)
137. Z. Liu, F. Huang, J. Du, W. Shu, H. Feng, X. Xu, Y. Chen, Rapid isolation of cancer cells using microfluidic deterministic lateral displacement structure. Biomicrofluidics **7**, 11801 (2013)
138. L.R. Huang, E.C. Cox, R.H. Austin, J.C. Sturm, Continuous particle separation through deterministic lateral displacement. Science **304**, 987–990 (2004)
139. N. Tottori, T. Nisisako, J. Park, Y. Tanagida, T. Hatsuzawa, Separation of viable and nonviable mammalian cells using a deterministic lateral displacement device. Biomicrofluidics **10**, 014125 (2016)
140. S. Choi, J.K. Park, Sheathless hydrophoretic particle focusing in a microchannel with exponentially increasing obstacle arrays. Anal. Chem. **80**, 3035–3039 (2008)
141. B. Kim, J.K. Lee, S. Choi, Continuous sorting and washing of cancer cells from blood cells by hydrophoresis. Bio. Chip J. (2015). https://doi.org/10.1007/s13206-016-0201-0
142. E. Sollier, D.E. Go, J. Che, D.R. Gosset, S. O'Byrne, W.M.M. Weaver, N. Kummer, M. Rettig, J. Goldman, N. Nickols, S. McCloskey, R.P. Kulkarni, D. Di Carlo, Size-selective collection of circulating tumor cells using Vortex technology. Lab Chip **14**, 63–77 (2014)
143. C.H. Hsu, D. Di Carlo, C. Chen, D. Irimia, M. Toner, Microvortex for focusing, guiding and sorting of particles. Lab Chip **8**, 2128–2134 (2008)
144. S. Song, S. Choi, Inertial modulation of hydrophoretic cell sorting and focusing. App. Phys. Let. **104**(7), 074106 (2014)
145. M. Madou, J. Zoval, G. Jia, H. Kido, J. Kim, N. Kim, Lab on a CD. Annu. Rev. Biomed. Eng. **8**, 601–628 (2006)
146. M. Yamada, M. Seki, Hydrodynamic filtration for on-chip particle concentration and classification utilizing microfluidics. Lab Chip **5**(11), 1233–1239 (2005)
147. R. Aoki, M. Yamada, M. Yasuda, M. Seki, In-channel focusing of flowing microparticles utilizing hydrodynamic filtration. Microfluid. Nanaofluid. **6**, 571–576 (2009)

148. M. Yamada, M. Nakashima, M. Seki, Pinched flow fractionation: continuous size separation of particles utilizing a laminar flow profile in a pinched microchannel. Anal. Chem. **76**(18), 5465–5471 (2004)
149. X. Lu, X. Xuan, Elasto-inertial pinched flow fractionation for continuous shape-based particle separation. Anal. Chem. **87**, 11523–11530 (2015)
150. X. Lu, X. Xuan, Continuous microfluidic particle separation via elasto-inertial pinched flow fractionation. Anal. Chem. **87**(12), 6389–6396 (2015)
151. G. Segre´, A. Silberberg, Radial particle displacements in poiseuille flow of suspensions. Nature **189**, 209–210 (1961)
152. D.R. Gossett, D. Di Carlo, Particle focusing mechanisms in curving confined flows. Anal. Chem. **81**, 8459–8465 (2009)
153. D. Di Carlo, Inertial microfluidics. Lab Chip **9**(21), 3038–3046 (2009)
154. J.S. Park, S.H. Song, H.I. Jung, Continuous focusing of microparticles using inertial lift force and vorticity via multi-orifice microfluidic channels. Lab Chip **9**(7), 939–948 (2009)
155. A.A.S. Bhagat, S.S. Kuntaegowdanahalli, I. Papautsky, Inertial microfluidics for continuous particle filtration and extraction. Microfluid. Nanofluid. **7**(2), 217–226 (2009)
156. J.F. Edd, D. Di Carlo, K.J. Humphry, S. Koester, D. Irimia, D.A. Weitz, M. Toner, Controlled encapsulation of single-cells into monodisperse picolitre drops. Lab Chip **8**, 1262–1264 (2008)
157. S.C. Hur, H.T. Tse, D. Di Carlo, Sheathless inertial cell ordering for extreme throughput flow cytometry. Lab Chip (2010). https://doi.org/10.1039/b919495a
158. J. Kim, J. Lee, C. Wu, S.M. Nam, D. Di Carlo, W. Lee, Inertial focusing in non-rectangular cross-section microchannels and manipulation of accessible focusing position. Lab Chip (2016). https://doi.org/10.1039/c5lc01100k
159. A. Berger, L. Talbot, L.S. Yao, Flow in curved pipes. Ann. Rev. Fluid Mech. **15**, 461–512 (1983)
160. A. Russom, A.K. Gupta, S. Nagrath, D. Di Carlo, J.F. Edd, M. Toner, Differential inertial focusing of particles in curved low-aspect-ratio microchannels. New J. Phys. **11**, 75025 (2009)
161. S.S. Kuntaegowdanahalli, A.A.S. Bhagat, G. Kumar, I. Papautsky, Inertial microfluidics for continuous particle separation in spiral microchannels. Lab Chip **9**, 2973–2980 (2009)
162. A.A.S. Bhagat, H.W. Hou, L.D. Li, C.T. Lim, J. Han, Dean flow fractionation (DFF) Isolation of circulating tumor cells (CTCs) from blood, in *Proceedings of 15th International Conference on Miniaturized Systems for Chemistry and Life Sciences*, October 28–November 1 2012, Okinawa, Japan (2012), pp. 524–526
163. G. Guan, L. Wu, A.A. Bhagat, Z. Li, P.C. Chen, S. Chao, C.J. Ong, J. Han, Spiral microchannel with rectangular and trapezoidal cross-sections for size based particle separation. Sci. Rep. **3**, 1475 (2013)
164. M.E. Warkiani, G. Guan, K.B. Luan, W.C. Lee, A.A. Bhagat, P.K. Chaudhuri, D.S. Tan, W. T. Lim, S.C. Lee, P.C. Chen, C.T. Lim, J. Han, Slanted spiral microfluidics for the ultra-fast, label-free isolation of circulating tumor cells. Lab Chip **14**, 128–137 (2014)
165. A.R. Pries, K. Ley, P. Gaehtgens, Generalization of the fahraeus principle for microvessel networks. Am. J. Physiol-Heart C **251**(6), H1324–H1332 (1986)
166. H.L. Goldsmith, G.R. Cokelet, P. Gaehtgens, Robin fahraeus: evolution of his concepts in cardiovascular physiology. Am. J. Physiol. **257**(Heart Circ. Physiol. 26):H1005–H1015 (1989)
167. Goldsmith HL (1971) Red cell motions and wall interactions in tube flow, in *Federation Proceedings*, vol. 30, pp. 1578–1588
168. E. Sollier, H. Rostaing, P. Pouteau, Y. Fouillet, J.L. Achard, Passive microfluidic devices for plasma extraction from whole human blood. Sens. Actuat. B-Chem. **141**, 617–624 (2009)
169. S.S. Shevkoplyas, T. Yoshida, L.L. Munn, M.W. Bitensky, Biomimetic autoseparation of Leukocytes from whole blood in a microfluidic device. Anal. Chem. **77**(3), 933–937 (2005)

170. H.W. Hou, A.A.S. Bhagat, A.G. Lin CHong, P. Mao, K.S. Wei Tan, J. Han, C.T. Lim, Deformability based cell margination—a simple microfluidic design for malaria-infected erythrocyte separation. Lab Chip **10**, 2605–2613 (2010)
171. Z. Shen, G. Coupier, B. Kaoui, B. Polack, J. Harting, C. Misbah, T. Podgorski, Inversion of hematocrit partition at microfluidic bifurcations. Microvasc. Res. **105**, 40–46 (2016)
172. R.D. Jaggi, R. Sandoz, C.S. Effenhauser, Microfluidic depletion of red blood cells from whole blood in high-aspect-ratio microchannels. Microfluid. Nanofluid. **3**, 47–53 (2006)
173. B. Alberts, A. Johnson, J. Lewis, M. Raff, K. Roberts, P. Walter, The cytoskeleton, in *Molecular Biology of the Cell*, 5rd edn. ed. Alberts (Garland Science, New York, 2008)
174. J.P. Mills, M. Diez-Silva, D.J. Quinn, M. Dao, M.J. Lang, K.S.W. Tan, C.T. Lim, G. Milon, P.H. David, O. Mercereau-Puijalon, S. Bonnefoy, S. Suresh, Effect of plasmodial RESA protein on deformability of human red blood cells harboring Plasmodium falciparum. Proc. Natl. Acad. Sci. U.S.A **104**(22), 9213–9217 (2007)
175. G.A. Barabino, M.O. Platt, D.K. Kaul, Sickle cell biomechanics. Ann. Rev. Biomed. Eng. **12**, 345–367 (2010)
176. M. Nishino, H. Tanaka, H. Oqura, Y. Inoue, T. Koh, K. Fujita, H. Sugimoto, Serial changes in leukocyte deformability and whole blood rheology in patients with sepsis or trauma. J. Trauma **59**(6), 1425–1431 (2005)
177. A.D. van der Meer, A.A. Poot, J. Feijen, I. Vermes, Analyzing shear stress-induced alignment of actin filaments in endothelial cells with a microfluidic assay. Biomicrofluidics **4** (1), 011103 (2010)
178. S. Suresh, J. Spatz, J.P. Mills, A. Micoulet, M. Dao, C.T. Lim, M. Beil, T. Seufferlein, Connectiones between single-cell biomechanics and human disease states: gastrointestinal cancer and malaria. Acta Biomater. (2005). https://doi.org/10.1016/j.actbio.2004.09.001
179. R.D. Gonza´lez-Cruz,V.C. Fonseca, E.M. Darling, Cellular mechanical properties reflect the differentiation potential of adipose-derived mesenchymal stem cells. Proc. Natl. Acad. Sci. U.S.A **109**(24), E1523 (2012)
180. S. Suresh, Biomechanics and biophysics of cancer cells. Acta Biomater. **3**, 413–438 (2007)
181. S.M.A. Haghparast, T. Kihara, J. Miyake, Distinct mechanical behavior of HEK293 cells in adherent and suspended states. Peer J (2015). https://doi.org/10.7717/peerj.1131
182. S.C. Hur, N.K. Henderson-MacLennan, E.R. McCabe, D. Di Carlo, Deformability-based cell classification and enrichment using inertial microfluidics. Lab Chip **11**, 912–920 (2011)
183. E.M. Darling, Force scanning: a rapid, high-resolution approach for spatial mechanical property mapping. Nanotechnology **22**, 175707 (2011)
184. N. Mohandas, E. Evans, Mechanical properties of the red cell membrane in relation to molecular structure and genetic defects. Ann. Rev. Biophys. Bio. **23**, 787–818 (1994)
185. R.E. Waught, P. Agre, Reductions of erythrocyte membrane viscoelastic coeffients reflect sprectrin deficiencies in hereditary spherocytosis. J. Clim. Invest. **81**, 133–141 (1988)
186. J. Guck, S. Schinkinger, B. Lincoln, F. Wottawah, S. Ebert, M. Romeyke, D. Lenz, H.M. Erickson, R. Ananthakrishnan, D. Mitchell, J. Ka¨s, S. Ulvick, C. Bilby, Optical deformability as an inherent cell marker for testing malignant transformation and metastatic competence. Biophys. J. **88**,3689–3698 (2005)
187. J.M.A. Mauritz, T. Tiffert, R. Seear, F. Lautenschlger, A. Esposito, V.L. Lew, J. Guck, C.F. Kaminskia, Detection of Plasmodium falciparum-infected red blood cells by optical stretching. J. Biomed. Opt. **15**(3), 030517 (2010)
188. H. Engelhart, E. Sackmann, On the measurement of shear elastic moduli and viscosities of erythrocyte plasma membranes by transient deformation in high frequency electric fields. Biophys. J. **54**, 495–508 (1988)
189. I. Doh, W.C. Lee, Y.H. Cho, A.P. Pisano, F.A. Kuypers, Deformation measurement of individual cells in large populations using a single-cell microchamber array chip. Appl. Phys. Lett. **100**, 173702 (2012)
190. E. Evans, R. Skalak, *Mechanics and thermodynamics of biomembranes* (Florida CRC Press, Boca Raton, 1980)

191. L.A. MacQueen, M.D. Buschmann, M.R. Wertheimer, Mechanical properties of mammalian cells in suspension measured by electro-deformation. J. Micromech. Microeng. **20**, 065007 (2010)
192. J. Chen, M. Abdelgawad, L.M. Yu, N. Shakiba, W.Y. Chien, Z. Lu, W.R. Geddie, M.A.S. Jewett, Y. Sun, Electrodeformation for single cell mechanical characterization. J. Micromech. Microeng. **21**, 054012 (2011)
193. G. Du, A. Ravetto, Q. Fang, J.M.J. den Toonder, Cell types can be distinguished by measuring their viscoelastic recovery times using a microfluidic device. Biomed. Microdevices **13**, 29–40 (2010)
194. Y.C. Kim, S.J. Park, J.K. Park, Biomechanical analysis of cancerous and normal cells based on bulge generation in a microfluidic device. Analyst **133**, 1432–1439 (2008)
195. D.R. Gosset, H.T.K. Tse, A.S. Lee, Y. Ying, A.G. Lindgreen, O.O. Yang, J. Rao, A.T. Clark, D. Di Carlo, Hydrodynamic stretching of single cells for large population mechanical phenotyping. Proc. Natl. Acad. Sci. U.S.A **109**, 7630–7635 (2012)
196. M. Gnerlich, S.F. Perry, S. Tatic-Lucic, A submersible piezoresistive MEMS lateral force sensor for a diagnostic biomechanics platform. Sens. Actuat. A-Phys. **188**, 111–119 (2012)
197. B. Barazani, S. Warnat, A. Fine, T. Hubbard, MEMS squeezer for the measurement of single cell rupture force, stiffness change, and hysteresis. J. Micromech. Microeng. **27**, 025002 (2017)
198. Lafitte N, Guillou H, Kumemura M, Jalabert L, Fujii T, Fujita H Collard D, Integrated MEMS platform with silicon nanotweezers and open microfluidic device for real-time and routine biomechanical probing on molecules and cells, in *35th Annual International Conference of the IEEE Engineering in Medicine and Biology Society* (EMBS 2013), Osaka, Japan (2013), pp. 148–151
199. A.M. Forsyth, J.D. Wan, W.D. Ristenpart, H.A. Stone, The dynamic behavior of chemically "stiffened" red blood cells in microchannel flows. Microvasc. Res. **80**, 37–43 (2010)
200. S.S. Lee, Y. Yim, K.H. Ahn, S.J. Lee, Extensional flow-based assessment of red blood cell deformability using hyperbolic converging microchannel. Biomed. Microdevices **11**, 1021–1027 (2009)
201. J.P. Shelby, J. White, K. Ganesan, P.K. Rathod, D.T. Chiu, A microfluidic model for single-cell capillary obstruction by Plasmodium falciparum infected erythrocytes. Proc. Natl. Acad. Sci. U.S.A **100**(25), 14618–14622 (2003)
202. H.W. Hou, Lee G.Y.H. LiQS, A.P. Kumar, C.N. Ong, C.T. Lim, Deformability study of breast cancer cells using microfluidics. Biomed. Microdevices **11**, 557–564 (2015)
203. Z.S. Khan, S.A. Vanapalli, Probing the mechanical properties of brain cancer cells using a microfluidic cell squeezer device. Biomicrofluidics **7**, 011806 (2013)
204. K.D. Nyberg, M.B. Scott, S.L. Bruce, A.B. Gopinath, D. Bikos, T.G. Mason, J.W. Kim, H. S. Choig, A.C. Rowat, The physical origins of transit time measurements for rapid, single cell mechanotyping. Lab Chip (2016). https://doi.org/10.1039/c6lc00169f
205. P. Preira, V. Grandne, J.M. Forel, S. Gabriele, M. Camara, O. Theodoly, Passive circulating cell sorting by deformability using microfluidic gradual filter. Lab Chip **13**, 161–170 (2013)
206. H. Bow, I.V. Pivkin, M. Diez-Silva, S.J. Goldfless, M. Dao, J.C. Niles, S. Suresh, J. Han, A microfabricated deformability-based flow cytometer with application to malaria. Lab Chip **11**, 1065–1073 (2011)
207. M. Mak, D. Erickson, A serial micropipette microfluidic device with applications to cancer cell repeated deformation studies. Integr. Biol. **5**, 1374–1384 (2013)
208. M.J. Rosenbluth, W.A. Lam, D.A. Fletcher, Analysing cell mechanics in hematologic diseases with microfluidic biophysical flow cytometry. Lab Chip **8**, 1062–1070 (2008)
209. W.A. Lam, M.J. Rosenbluth, D.A. Fletcher, Chemotherapy exposure increases leukemia cell stiffness. Blood **109**(8), 3505–3508 (2007)
210. T. Herricks, M. Antia, P.K. Rathod, Deformability limits of Plasmodium falciparum-infected red blood cells. Cell. Microbiol. **11**(9), 1340–1353 (2009)
211. J. Picot,P.A. Ndour, S.D. Lefevre, W. El Nemer, H. Tawfik, J. Galimand, L. Da Costa, J.A. Ribeil, M. de Montalembert, V. Brousse, B. Le Pioufle, P. Buffet, C. Le Van Kim, O.

Français, A biomimetic microfluidic chip to study the circulation and mechanical retention of red blood cells in the spleen. Am. J. Hematol. (2015). https://doi.org/10.1002/ajh.23941
212. S. Huang, A. Undisz, M. Diez-Silva, H. Bow, M. Dao, J. Han, Dynamic deformability of Plasmodium falciparum-infected erythrocytes exposed to artesunate in vitro. Integr Biol **5**, 414–422 (2013)
213. A. Adamo, A. Sharei, L. Adamo, B. Lee, S. Moa, K.F. Jensen, Microfluidics-based assessment of cell deformability. Anal. Chem. **84**, 6438–6443 (2012)
214. M. Abkarian, M. Faivre, H.A. Stone, High-speed microfluidic differential manometer for cellular-scale hydrodynamics. Proc. Natl. Acad. Sci. U.S.A **103**(3), 538–542 (2006)
215. M. Abkarian, M. Faivre, R. Horton, K. Smistrup, C.A. Best-Popescu, H.A. Stone, Cellular-scale hydrodynamics. Biomed. Mater. **3**, 034011 (2008)
216. Q. Guo, S.J. Reiling, P. Rohrbach, H.S. Ma, Microfluidic biomechanical assay for red blood cells parasited by Plasmodium falciparum. Lab Chip **12**, 1143–1150 (2012)
217. B.M. Cooke, N. Mohandas, R.L. Coppel, The malaria-infected red blood cell: structural and functional changes. Adv. Parasit. **50**, 1–86 (2001)
218. S.B. Huang, Z. Zhao, D.Y. Chen, H.C. Lee, Y.N. Luo, T.K. Chiu, J.B. Wang, J. Chen, M.H. Wu, A clogging-free microfluidic platform with an incorporated pneumatically-driven membrane-based active valve enabling specific membrane capacitance and cytoplasm conductivity characterization of single cells. Sens. Actuat. B Chem. **190**, 928–936 (2014)
219. W. Beattie, X. Qin, L. Wang, H. Ma, Clog-free cell filtration using resettable cell traps. Lab Chip **14**, 2657–2665 (2014)
220. Y. Zheng, E. Shojaei-Baghini, A. Azad, C. Wang, Y. Sun, High-throughput biophysical measurement of human red blood cells. Lab Chip **12**, 2560–2567 (2012)
221. O. Otto, P. Rosendahl, A. Mietke, S. Golfier, C. Herold, D. Klaue, S. Girardo, S. Pagliara, A. Ekpenyong, A. Jacobi, M. Wobus, N. Tpfner, U.F. Keyser, J. Mansfeld, E. Fischer-Friedrich, J. Guck, Real-time deformability cytometry: on-the-fly cell mechanical phenotyping. Nat. Methods (2015). https://doi.org/10.1038/nmeth.3281
222. M. Xavier, P. Rosendahl, M. Herbig, M. Krater, D. Spencer, M. Bornhauser, R.O.C. Oreffo, H. Morgan, J. Guck, O. Otto, Mechanical phenotyping of primary human skeletal stem cells in heterogeneous populations by real-time deformability cytometry. Integr. Biol. **8**, 616–623 (2016)
223. Y. Deng, A.J. Chung, Next generation deformability cytometry: fully automated, high-throughput and near real-time cell mechanotyping, in *Proceedings of 20th International Conference on Miniaturized Systems for Chemistry and Life Sciences*, 9–13 Oct 2016, Dublin, Ireland (2016), pp. 148–149
224. J. Chen, Y. Zheng, Q.Y. Tan, E. Shojaei-Baghini, Y.L. Zang, J. Li, P. Prasad, L.D. You, X. Y. Wu, Y. Sun, Classification of cell types using a microfluidic device for mechanical and electrical measurement on single cells. Lab Chip **11**, 3174–3181 (2012)